Forest Ecology and Management 583 (2025) 122576

Contents lists available at ScienceDirect

Forest Ecology and Management

journal homepage: www.elsevier.com/locate/foreco

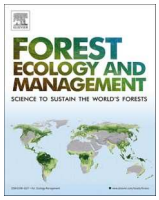

Moderate-resolution mapping of aboveground biomass stocks, forest structure, and composition in coastal Alaska and British Columbia☆

James Lamping [a,*], Melissa Lucash [a], David M. Bell [b], Daniel R. Irvine [b], Matt Gregory [c]

[a] Department of Geography, University of Oregon, Eugene, OR 97403, United States
[b] Pacific Northwest Research Station, USDA Forest Service, Corvallis, OR 97331, United States
[c] Department of Forest Ecosystems and Society, Oregon State University, Corvallis, OR 97331, United States

ARTICLE INFO

Keywords:
Temperate Rainforest
Forest structure
Gradient nearest neighbor
Landsat
Imputation
National Forest Inventories

ABSTRACT

The forests of coastal Alaska and British Columbia are globally significant for their high carbon storage capacity and complex forest structure, hosting some of the densest values of aboveground biomass in the world. These ecosystems support biodiversity, provide critical habitat, and serve as long-term carbon sinks, offering resilience to climate change. However, comprehensive, spatially continuous estimates of forest structure across this region have been limited, particularly across political boundaries. In this study, we used a Gradient Nearest Neighbor (GNN) modeling approach to integrate extensive forest inventory plot data with satellite-derived environmental variables. This approach enabled us to produce moderate-resolution (30-meter) maps of aboveground biomass, species biomass, forest age, basal area, and additional structural attributes. Our results indicated that climate and topography accounted for the majority of the explainable variation across all modeling regions. Predictions of aboveground live biomass were higher than previous estimates, particularly in Southeast Alaska, where estimates were 30–53 % greater than previous studies. Forest structure varied across the region, with older forests found in Southeast Alaska and higher tree densities in British Columbia. Collectively, the coastal forests of Alaska and British Columbia store approximately 3.58 petagrams of carbon. These spatially explicit maps offer critical insights for carbon monitoring, forest management, and biodiversity conservation across this ecologically diverse and politically fragmented landscape.

1. Introduction

Today's most pressing challenges in natural resource management and conservation planning extend across vast spatial scales, often traversing political boundaries, land ownerships, administrative jurisdictions, and intricate ecological gradients. A multitude of interacting threats, such as wildfires, invasive species, and climate change, alongside balancing various benefits like wildlife habitat preservation, watershed health, and timber supply (DeGayner et al., 2005; Shanley et al., 2015) necessitates an accurate and complete understanding of our forested systems that traverses these human boundaries and environmental gradients. Consequently, there is a growing demand among analysts and decision-makers for comprehensive, highly detailed, and spatially-complete data on vegetation and land cover. Maps of vegetation structure and composition are helpful for land managers to delineate potential habitat for wildlife (Vogeler and Cohen, 2016), understand natural disturbance regimes (Kennedy et al., 2014), and estimate carbon stocks. They can also be useful for modelers, as baseline conditions for projecting changes in the environment due to climate change (Lucash et al., 2023). However, in remote regions of the world, these maps may be either too coarse or completely lacking altogether (Fassnacht et al., 2024).

One such area is the forests of the Pacific coast of North America, which include nearly 30 % of all temperate rainforests on Earth (Veblen and Alaback, 1996). These forests are globally significant for their role in storing and cycling carbon and are home to some of the highest aboveground carbon densities in the world (Alaback, 1996; Yatskov et al., 2019). Regionally and locally, they are valued for their ability to provide ecosystem services and their cultural significance by Indigenous communities, playing a crucial role in supporting regional economies (e.g. timber, berry and salmon production; Crone and Mehrkens, 2013). They are described as being among the most intact tracts of coastal

☆ Planned Submission to Remote Sensing and Environment

* Corresponding author.
E-mail address: jlamping@uoregon.edu (J. Lamping).

https://doi.org/10.1016/j.foreco.2025.122576
Received 4 November 2024; Received in revised form 27 January 2025; Accepted 14 February 2025
Available online 27 February 2025

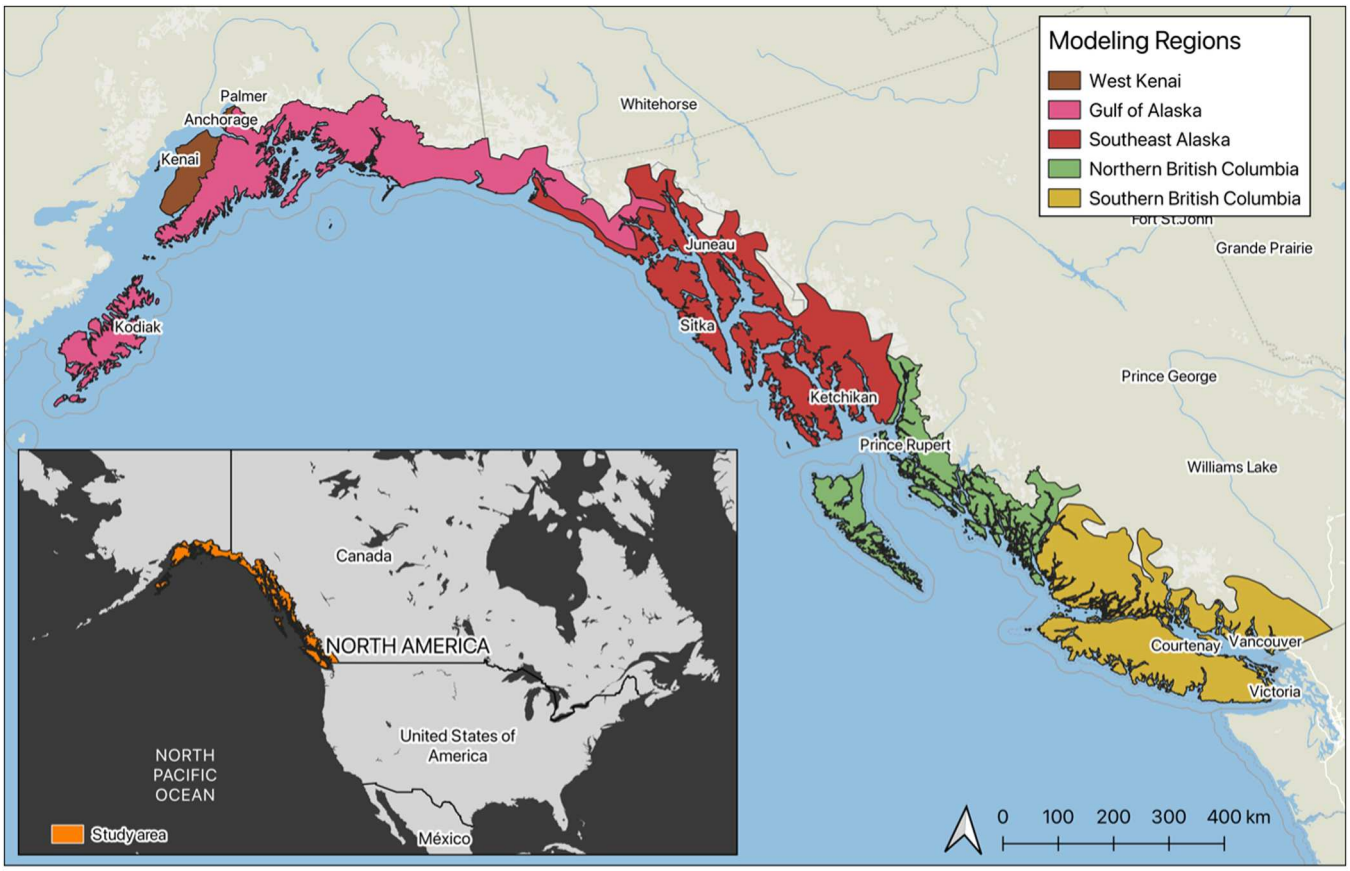

Fig. 1. GNN modeling region of the temperate rainforests of North America separated into five sub-modeling regions.

temperate rainforests in the world (Alaback, 1996; DellaSala et al., 2022, 2011; Suttles et al., 1997). Yet despite their global and regional significance, there is a relative lack of consistent, cross-boundary, spatial data at resolutions appropriate for informing monitoring efforts and management decisions across the temperate rainforests of North America.

Efforts to map these forests encounter obstacles such as limited spatial and temporal coverage, sampling bias, and the high cost and labor of data collection (McRoberts and Westfall, 2014). Networks of ground observations in these remote regions lack the granularity needed to capture the complex and heterogeneous nature of these forested regions, where variations in topography, climate, and species composition are pronounced (Beamish et al., 2020; Bidlack et al., 2017; Kane et al., 2008). Field surveys provide highly accurate and detailed data at specific locations. However, due to the time-consuming, labor-intensive, and expensive nature of data collection, only a small fraction of vast geographic areas can be practically surveyed. Furthermore, remote areas, such as designated Wilderness Areas, often lack permanent plot support and infrequent remeasurement periods, making monitoring change in these systems challenging (Bidlack et al., 2017).

To address these limitations, researchers have increasingly combined field-sampled forest structure data with satellite imagery, which is spatially complete, spectrally consistent, frequently remeasured, and often available for free (Banskota et al., 2014; Ohmann and Gregory, 2002; Wulder et al., 2012). This combination has allowed for comprehensive estimates of forest structure over large areas, mitigating issues such as high costs, limited spatial coverage, and long intervals between repeated measurements of traditional field-based inventories (Lister et al., 2020; White et al., 2016). Some methods focus on extrapolating localized data obtained from field samples across entire regions using statistical predictive modeling, such as linear regression, Random Forest (RF), and gradient nearest neighbor (GNN) imputation (Krebs et al., 2019; Matasci et al., 2018; Zald et al., 2016). These approaches relate localized forest measurements to multispectral images and other geospatial datasets to facilitate forest structure and composition mapping. The integration of field data and satellite imagery thus provides an effective solution for creating comprehensive forest structure estimates, enhancing the accuracy and efficiency of forest inventory and management practices.

A significant challenge in forest research and management has been the lack of harmonized datasets that bridge multiple forest inventory systems across political boundaries. Our study integrates datasets from two national inventory systems—the USDA Forest Service Forest Inventory and Analysis (FIA) program and the Forest Analysis Inventory Branch (FAIB) in British Columbia—into a unified, cross-border framework. This integration represents a novel effort to reconcile differences in inventory methodologies, creating a unified, cross-border training dataset that enables consistent analysis of forest structure and composition. We then created a cloud-free and terrain-corrected satellite composite of the entire region, combining it with continuous environmental layers such as climate, disturbance, and landcover type. Field data were integrated with remotely-sensed data using a Gradient Nearest Neighbor (GNN) imputation technique, which models forest attributes through Canonical Correspondence Analysis (CCA) and imputes results across the landscape based on Euclidean distances (Ohmann and Gregory, 2002). This method enables the mapping of various forest attributes across a broad geographic area and allows for the imputation of any forest attribute derived from field observations to similar pixels throughout the landscape.

Several spatially explicit datasets of forest structure and composition exist for Canada and Alaska. For instance, Canada has national-scale maps of biomass, forest structure, tree species distributions, and forest

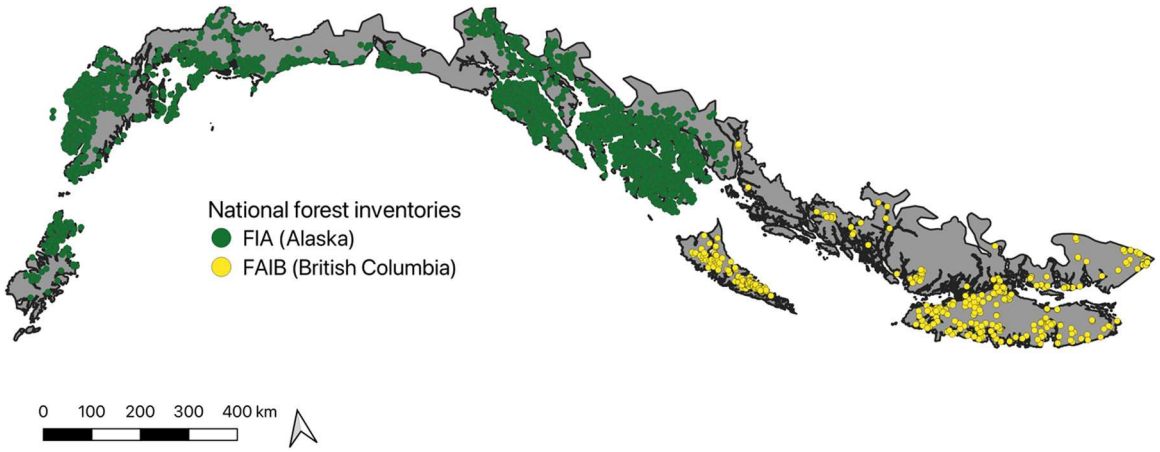

Fig. 2. Plot location by country of origin, with FIA plot locations labeled in green and FAIB plot locations in yellow. FIA plot locations are shown here using the publicly available fuzzed coordinates.

age (e.g., Hermosilla et al., 2022; Maltman et al., 2023; Matasci et al., 2018). Alaska also has datasets focused on tundra and Arctic vegetation and aboveground biomass (e.g., Berner et al., 2018). While these datasets provide valuable insights, they are often limited to specific geographic areas. In contrast, our study integrates the Gradient Nearest Neighbor (GNN) imputation method with a harmonized, cross-boundary training dataset, combining multiple forest inventory systems from both Canada and the United States. This represents a novel approach for addressing data gaps and achieving consistency in mapping forest structure and composition across the transboundary region of the North American temperate rainforest.

The goal of this study was to improve our understanding of forest composition and structure across the coastal temperate rainforests of Alaska and British Columbia by developing spatially explicit maps that integrate cross-border forest inventory data. To achieve this goal, our objectives were to: (1) create spatially explicit, cross- border, predictions of forest biomass, forest composition, and structural metrics including aboveground biomass, forest age, basal area, and volume using field inventory data, with predictors derived from multispectral, climate, disturbance, and landcover maps; (2) determine the environmental variables that have the strongest influence on the spatial patterns of aboveground biomass, basal area, density, and volume of live and dead trees across the region; (3) benchmark the forest biomass stock predictions against regional and global estimates; and (4) assess the modeled outputs to identify environmental gradients that may require additional plot support to improve representation.

2. Methods

2.1. Study area

The study area for this project spans nearly 29.9 million hectares of coastal regions of coastal British Columbia up through Southeast Alaska to Kodiak Island (Fig. 1). It spans large climatic, physiographic, geologic, and vegetation gradients with a latitudinal gradient of 48°N to 61°N and a longitudinal gradient of 121°W to 154°W. The forests in this region experience a maritime climate characterized by mild temperatures, high humidity, and abundant precipitation throughout the year, supporting some of the highest amounts of above- and belowground biomass in the world (Buma et al., 2016; McNicol et al., 2019). Winters are mild, with temperatures ranging from 0°C to 10°C, accompanied by substantial rainfall and occasional snowfall in the southern extents, with increasing amounts of snow with increasing latitude and elevation. Springs bring increasing temperatures and abundant rain showers, while summers remain cool with temperatures ranging from 15°C to 25°C and persistent fog and mist.

The study area was split into five separate modeling regions based on climatic differences, administrative boundaries, and species composition. The western Kenai Peninsula and the Anchorage Bowl comprise portions of the Cook Inlet Basin and represent a transition to the boreal forest biome, characterized by cooler winters, warmer summers, and far less annual precipitation than the temperate maritime region (Nowacki et al., 2003). In contrast, modeling regions within the temperate coastal rainforest are characterized generally by warmer winters and cooler summers, with substantial annual precipitation. Alaska comprises two temperate modeling regions: the Southcentral region, which surrounds the Gulf of Alaska, and the Southeast region, which encompasses the Tongass National Forest. Coastal British Columbia was split into two separate modeling regions as well, with the northern extent of the Douglas-fir range as the boundary between the two (Hermann and Lavender, 1990).

2.2. Forest plot data

Forest inventory data were obtained and combined from both the United States and British Columbia (Fig. 2). In British Columbia, we utilized sample plots from the Forest Analysis and Inventory Branch (FAIB; Government of British Columbia, 2023) while in Alaska plot data was obtained from the USDA Forest Service Forest Inventory and Analysis Program (FIA; Gray et al., 2012). The two inventories have somewhat different purposes, with FIA measuring vegetation in permanent plots on forested lands across the United States while the FAIB database helps determine an appropriate annual allowable cut (AAC) for the timber harvest regions of British Columbia. The USDA FIA uses a systematic grid of permanent plots that are approximately 1 hectare in size, with four subplots, and data are collected on trees greater than 5 in. in diameter at breast height (DBH). British Columbia's FAIB, on the other hand, uses a mix of fixed-radius (0.01 ha in size) and variable-radius plot designs, often focusing on commercial species. For both datasets, plots were filtered to the latest remeasurement date and trees that were greater than 12.7 cm DBH, with plot collection dates ranging between 2004 and 2019. There were multiple plots within the FAIB dataset that contained the same coordinates ($n = 42$), and these plots were also removed from analysis. Variable radius plots from the FAIB database were also omitted from the analysis to maintain consistency between the two different inventory systems. In total, 2755 plot observations were used, with 2074 from FIA and 681 from FAIB.

To calculate individual tree-level biomass across both datasets, Kozak stem taper equations (Kozak et al., 1969) were used to estimate the total volume of each standing stem. The Kozak taper equations were selected for several reasons. Firstly, it was discovered that the component ratio method (CRM) used by the FIA (Woodall et al., 2011) has

Table 1
Forest composition and structural data obtained from forest plot observations.

Variable code	Units	Description
total_bio	$g \cdot m^{-2}$	plot level aboveground tree biomass density
snag_bio	$g \cdot m^{-2}$	Plot level biomass of standing dead trees
species _gm2	$g \cdot m^{-2}$	species specific biomass densities $g \cdot m^{-2}$ (Table 2)
BA_GE_3	$m^2 \cdot hectare^{-1}$	Basal area of live trees
BAC_GE_3	$m^2 \cdot hectare^{-1}$	Basal area of live conifers
BAH_GE_3	$m^2 \cdot hectare^{-1}$	Basal area of live hardwoods
TPH_live	$trees \cdot hectare^{-1}$	Density of live trees
TPH_dead	$trees \cdot hectare^{-1}$	Density of dead trees
TPH_Con	$trees \cdot hectare^{-1}$	Density of live conifers
TPH_Hw	$trees \cdot hectare^{-1}$	Density of live hardwoods
VPH_live	$m^3 \cdot hectare^{-1}$	Volume of live trees
VPH_dead	$m^3 \cdot hectare^{-1}$	Volume of dead trees
VPH_Con	$m^3 \cdot hectare^{-1}$	Volume of live conifers
VPH_Hw	$m^3 \cdot hectare^{-1}$	Volume of live hardwoods
AGE_DOM	years	95th percentile of tree ages
QMD_live	cm	Quadratic mean diameter of all live trees

Table 2
Tree species included in study.

Species	*Species Code*	*Common name*
Abies amabilis	11	pacific silver fir
Abies grandis	17	grand fir
Abies lasiocarpa	19	subalpine fir
Chamaecyparis nootkatensis	42	Alaska yellow cedar
Picea glauca	94	white spruce
Picea mariana	95	black spruce
Picea sitchensis	98	Sitka spruce
Pinus contorta	108	lodgepole pine
Pinus monticola	119	western white pine
Pseudotsuga menziesii	202	Douglas-fir
Taxus brevifolia	231	Pacific yew
Thuja plicata	242	western redcedar
Tsuga heterophylla	263	western hemlock
Tsuga mertensiana	264	mountain hemlock
Acer macrophyllum	312	bigleaf maple
Alnus rubra	351	red alder
Betula papyrifera	375	paper birch
Populus tremuloides	746	quaking aspen
Populus trichocarpa	747	black cottonwood

potentially been underestimating individual tree biomass (Chojnacky et al., 2014; Westfall et al., 2024). Secondly, the Kozak equations were specifically developed for the region to estimate tree volume and account for trees with broken tops. Tree stem volume was then converted to standing biomass with species-specific wood densities (Jenkins et al., 2003). After converting individual tree biomass to unit/area densities via the supplied expansion factors, plot data was reassessed for erroneous biomass densities at whole-plot level. Plots with biomass densities well outside the known range of upper biomass limits for the region ($n = 94$) were omitted from the analysis (Buma et al., 2016; Krumlik, 1974; Smithwick et al., 2002). Forest structural attributes, found in Table 1, were then summarized for each plot.

2.3. Gradient nearest neighbor predictions

To model forest composition and structure across all forested land within the study area, we used Gradient Nearest Neighbor (GNN) imputation as described in Ohmann et al., (2011) and Ohmann and Gregory, (2002). The GNN imputation modeling method was chosen due to its robustness to the nonlinear responses expected of vegetation communities to environmental gradients and to the response matrices containing many null values and without normal distributions, which is common in plant community ecology. This arises from the use of the constrained ordination method called canonical correspondence analysis (CCA; Ter Braak, 1986) as the basis for relating the multivariate

Table 3
Environmental predictor variables that will be used in GNN mapping.

Predictor	Band name	Description
Landsat 8 Composite	blue	Landsat 8 blue band
	green	Landsat 8 green band
	red	Landsat 8 red band
	NIR	Landsat 8 near infrared band
	SWIR1	Landsat 8 shortwave infrared 2 band
	SWIR2	Landsat 8 shortwave infrared 1 band
Landsat 8 indices	R54	Landsat 8 near infrared band / Landsat 8 red band
	R65	Landsat 8 shortwave infrared 1 / Landsat 8 near infrared
	R67	Landsat 8 shortwave infrared 1 / Landsat 8 shortwave infrared 2
	NDVI	Landsat 8 normalized difference vegetation index
Landsat 8 Tasseled Cap	brightness	Axis 1 from tasseled cap transformation of Landsat 8 surface reflectance.
	greenness	Axis 2 from tasseled cap transformation of Landsat 8 surface reflectance.
	wetness	Axis 3 from tasseled cap transformation of Landsat 8 surface reflectance.
Landcover	landcov	National Land Cover Database (NLCD) Landcover classifications
Topography	elevation	Elevation (m)
	slope	Slope (degrees)
Location	latitude	Northing based on EPSG:3338 (m)
	longitude	Easting based on EPSG:3338 (m)
Climate	bio1	Mean annual air temperature
	bio4	Temperature seasonality (°C/100)
	bio5	Mean daily air temperature of the warmest month (°C)
	bio12	Annual precipitation amount ($kg \cdot m^{-2}$)
	bio14	Precipitation amount of the driest month ($kg \cdot m^{-2}$)
	bio15	Precipitation seasonality ($kg \cdot m^{-2}$)
Disturbance	TSD	Time since disturbance obtained from Landtrendr (Kennedy et al., 2010)

forest inventory data to geospatial predictors. CCA is best suited to community datasets where (1) species responses to the environment are unimodal and (2) the important underlying environmental variables have been measured. Because CCA uses data on the environment to structure the community analysis, and CCA plots points in a space defined by environmental variables, CCA can be considered a "direct gradient analysis" method.

To map forest attributes (Table 1), along with species specific biomass densities (Table 2), we imputed the mean of the five plots most similar to each 30-m pixel (spatial grain of predictor variables; see Section 2.3.1) based on the CCA model results. The selection of the five nearest neighbors for each pixel was based on the weighted Euclidean distance within multivariate gradient space between a pixel environmental values and those observed at a plot location. We chose to impute the mean of the five nearest neighbors because previous research on nearest neighbor imputation indicated that imputing the mean of several neighbors can result in improved prediction accuracy for individual forest structure variables compared to using only the nearest neighbor (Bell et al., 2023; Chirici et al., 2016; McRoberts, 2012). For each modeling region, we utilized plot data within the region and any directly neighboring regions. Due to the low plot support in portions of the Northern BC region, we also included plots from Southeast Alaska when modeling the Southern BC region. A total of 693 plot observations were used for the western Kenai region, 1831 plots for Southcentral Alaska, 2066 plots for Southeast Alaska, 2053 plots for the northern region of coastal British Columbia, and 2053 plots for the southern region of coastal British Columbia. This approach enhanced plot support for each region and helped minimize the introduction of artificial boundaries in our results.

2.3.1. Mapped explanatory data

The explanatory variables used in the GNN imputation were continuous raster layers describing observed satellite reflectance values, topography, climate, landcover, location, and disturbance (Table 3). All layers were sampled to the same resolution (30 m) and extent using the terra package (Hijmans, 2023) in R (R Core Team, 2023). Depending on if the predictor variable was categorical or continuous, the resampling method used was either accomplished using bilinear interpolation or nearest neighbor respectively. A cloud-free and terrain-corrected Landsat 8 composite, calibrated for surface reflectance, was generated in Google Earth Engine (GEE; Gorelick et al., 2017) using a modified version of an image pre-processing tool developed by Hurni et al., (2017). This version replaces SRTM elevation data with JAXA ALOS elevation data due to data availability at high latitudes (Tadono et al., 2016). The Landsat 8 image collection was filtered to months with minimal snow cover (May-August). The CFMASK algorithm in GEE was employed to assess pixel quality, enabling the exclusion of cloud edges and shadows and assigned reflectance was determined by calculating the median value of each pixel within the annual time series. Images used were captured between 2016 and 2021, with priority given to pixels that were captured in 2018.

In addition to individual spectral bands, Tasseled Cap transformations (TCT) were calculated based on the Landsat imagery, providing a set of spectral indices effective at capturing changes in the density and vigor of vegetative foliage (Greenness), surface reflectance from the particles that make up the bare earth (Brightness), and surface moisture (Wetness) (Crist and Cicone, 1984). TCT condenses the multidimensional spectral data into a few key components that simplify the complex spectral information, facilitating the analysis of land cover changes, vegetation health, and ecosystem monitoring (Cohen and Goward, 2004).

To represent areas that have been disturbed in the past the Landsat-based detection of Trends in Disturbance and Recovery (LandTrendr) algorithm, implemented in GEE, was used (Kennedy et al., 2018, 2010). LandTrendr exploits time-series satellite imagery to detect and characterize land cover changes over time. It was developed to analyze time series data from Landsat satellite imagery, focusing on identifying and quantifying disturbances (like logging, fires, or storms) and subsequent recovery processes. It uses a pixel-based approach to identify temporal trends and abrupt changes in spectral characteristics and is particularly useful for assessing long-term trends and disturbances in large-scale ecosystems. LandTrendr was used to detect disturbed pixels across the entire continuous Landsat collection (1985 – 2021). To ensure disturbance from harvests were fully represented, historical harvest boundaries (Forest Analysis and Inventory Branch, 2023; USDA, 2022) were added to the LandTrendr output of disturbed pixels providing a layer that represents the time since disturbance (2021 – *year of disturbance*) for both human and natural causes.

Climate, landcover, and topographic layers were also included due to their influence on observed vegetation patterns found in northwest forests (Ohmann and Spies, 1998). Downscaled climatology's were derived from CHELSA V2.1 (Karger et al., 2017) while topographic layers, such as elevation and slope, were developed from JAXA ALOS (Tadono et al., 2016). Landcover classes (NLCD) from the Multi-Resolution Land Characteristics (MRLC) Consortium were used as predictors of vegetation type and as a tool to mask non-forested areas from this analysis. Developed and barren areas were masked from analysis.

2.4. Model evaluation

To evaluate CCA model performance at individual sites, we compared a subset of predicted values to observed values using a modified-leave-one-out-cross-validation. This was done for each individual modeling region, and then again for all modeling regions to show overall agreement across the study area. For each of the compared vegetation attributes, the 6 nearest neighbors were predicted. The first nearest neighbor was omitted, being that it would represent the observed site we are comparing to, and the mean of the second- through sixth-nearest neighbor was calculated. This has been used in previous studies as a computationally efficient method similar to leave-one-out-cross-validation (Ohmann and Gregory, 2002). Statistical comparisons were used to quantify how well the models predicted observed values and if there were any trends in systematic and unsystematic bias (Riemann et al., 2010). To assess the relationship between observed and predicted values, we used a geometric mean functional relationship (GMFR) regression to account for errors. We compared this to the 1:1 line which represents perfect agreement between observed and predicted data. Systematic and unsystematic errors were characterized by agreement coefficients (ACsys and ACuns). To evaluate how well the

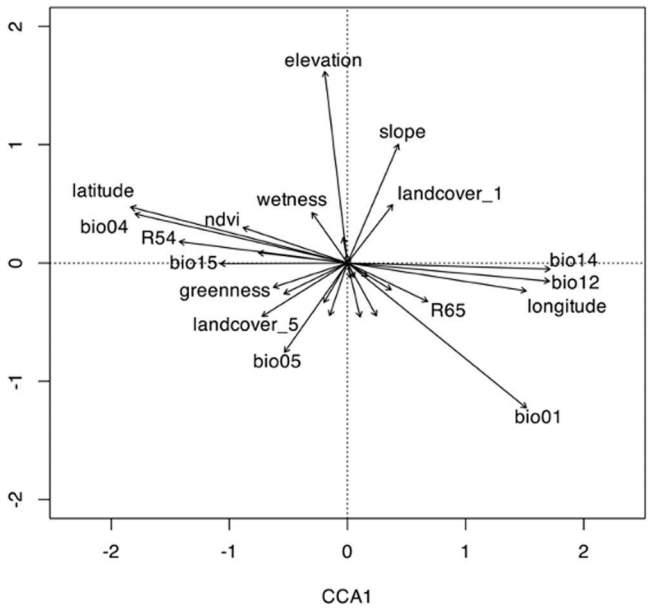

Fig. 3. Associations between vegetation and explanatory variables from canonical correspondence analysis for the Tongass modeling region. The arrow length represents the strength of the correlation between the environmental variables and the plot forest structure.

Table 4
Variation explained by subsets of variables in canonical correspondence analysis.

	Percent variation explained by modeling region				
Grouped Explanatory variables	West Kenai	Gulf of AK	Southeast AK	Northern BC	Southern BC
Climate	18.7 %	9.2 %	7.3 %	8.1 %	9.5 %
Topography	13.1 %	8.5 %	8.1 %	8.0 %	9.1 %
Spectral	15.0 %	6.2 %	7.0 %	5.3 %	5.5 %
Tasseled Cap	7.7 %	2.7 %	2.6 %	6.3 %	6.4 %
Climate + **Topography**	23.3 %	12.2 %	10.6 %	11.9 %	12.5 %
Topography + **Spectral**	25.2 %	12.5 %	12.6 %	12.4 %	13.5 %
Tasseled Cap + Spectral	15.2 %	6.3 %	7.0 %	7.9 %	8.2 %
Climate + **Topography** + **Spectral**	29.9 %	15.9 %	15.1 %	15.1 %	15.4 %
Climate + **Topography** + **Tasseled Cap**	26.7 %	13.9 %	12.6 %	15.8 %	15.7 %
All predictor groups	30.0 %	16.0 %	15.1 %	16.5 %	16.8 %

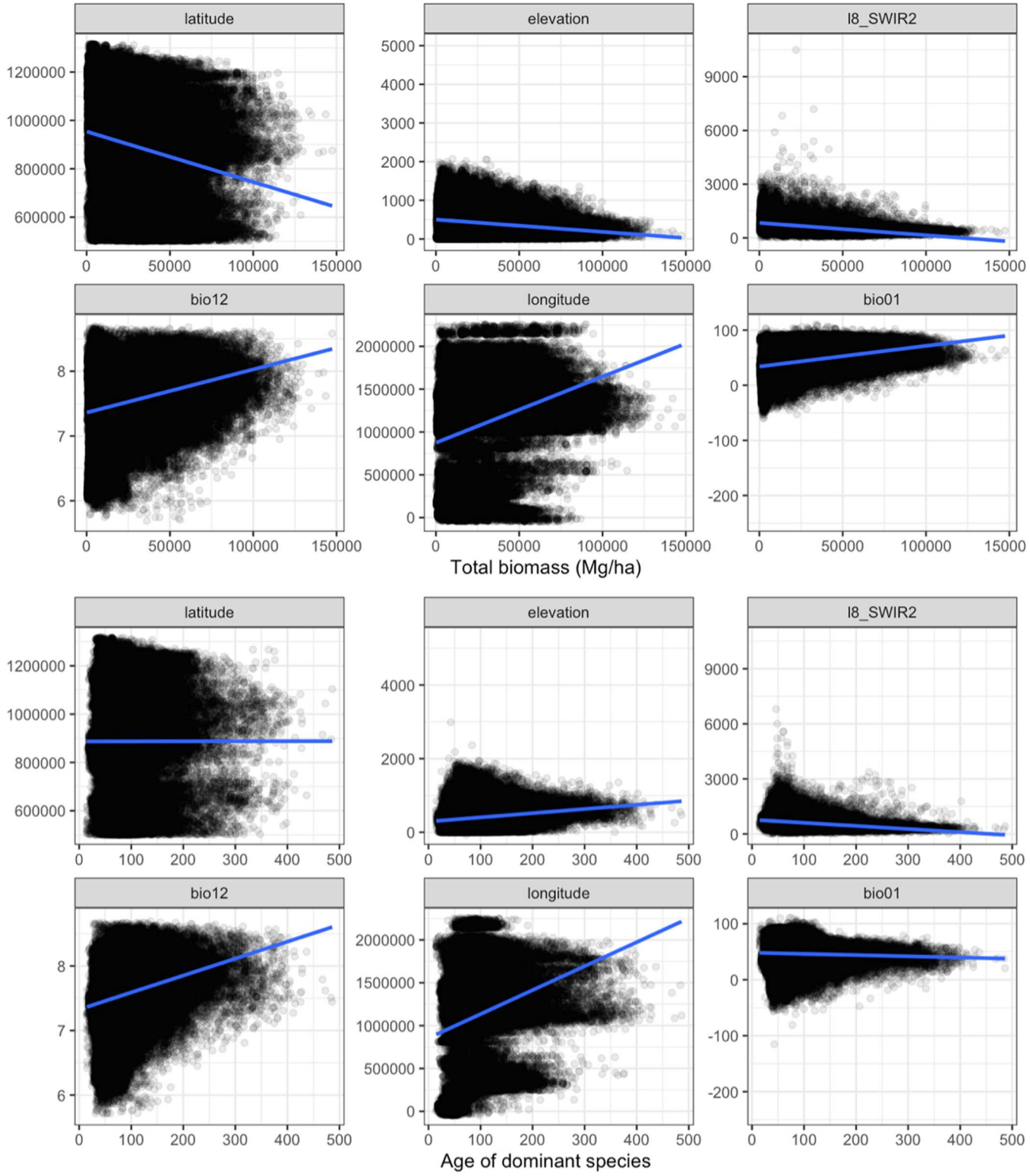

Fig. 4. Regressions of aboveground live biomass (top) and age of dominant species (bottom) to environmental variables shown to have strong influence on model outcomes based on CCA results.

model classified individual species extents, we reported accuracy (Acc), balanced accuracy (ACC_b), as well as omission and commission error. (Olofsson et al., 2014; Sokolova and Lapalme, 2009).

As noted above, maps were generated based on the mean of the five nearest-neighbor distances, creating a spatial representation of how well the conditions characterized by the predictor variables in each pixel are represented in the training dataset. Pixel values in this map represent the mean Euclidean distances from the environmental gradients a pixel represents to the nearest neighbors imputed by GNN. While this is not a true measure of uncertainty, it highlights areas where the environmental conditions in the training dataset may not fully capture the variability present in the broader landscape (Ohmann and Gregory, 2002; Ohmann

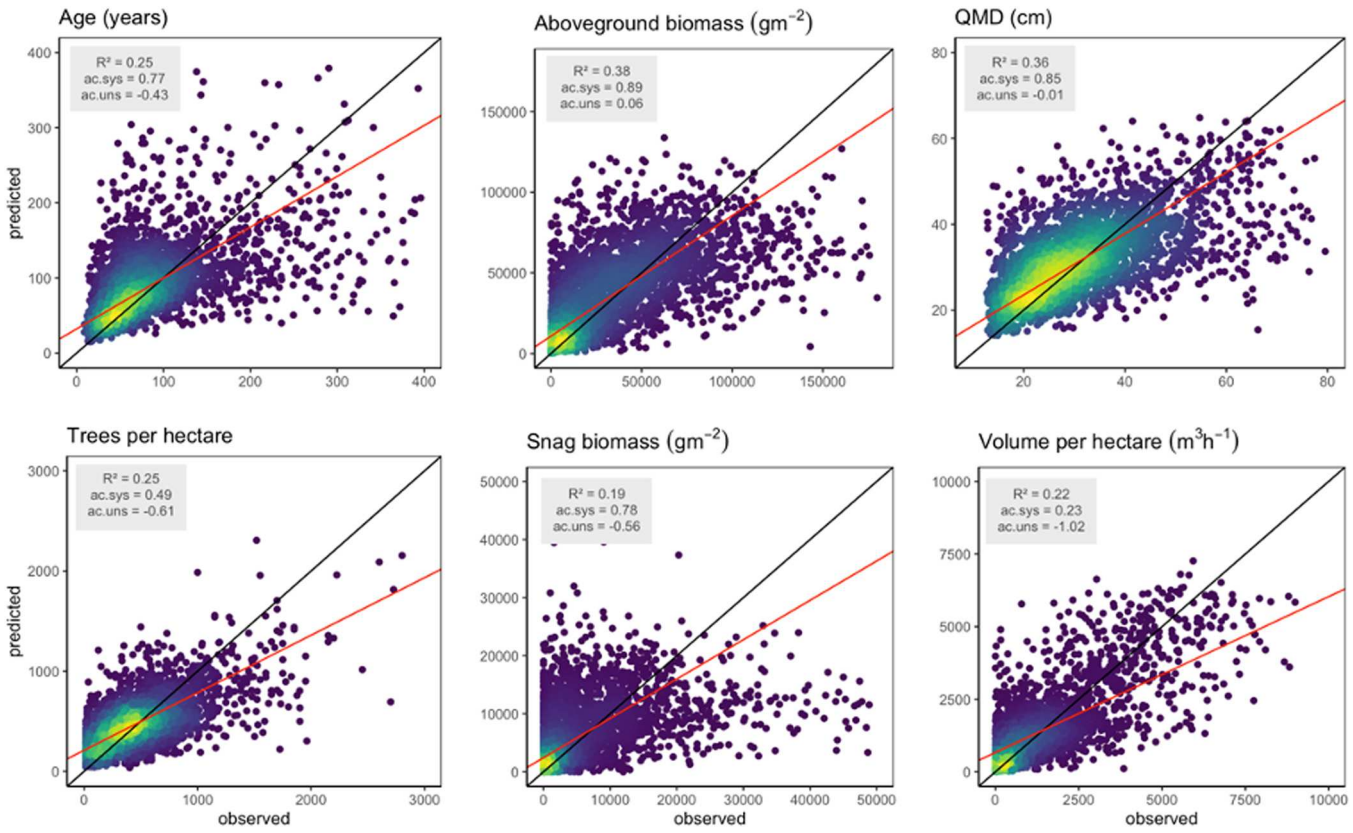

Fig. 5. Comparison of predicted to observed data from the leave-one-out cross-validation analysis. Displayed is the 1:1 line with the GMFR line plotted in red. Data points are colorized by density to surrounding points, with yellow illustrating areas of highest point density.

et al., 2011; Moeur and Stage, 1995).

3. Results

3.1. Explanatory variables relationship to plot data

Environmental variables, such as elevation, slope, location, and climate, all had a strong influence on forest biomass, structure, and species composition (Fig. 3). However, the performance of explanatory variables in predicting forest structure varied across the different modeling regions (Table 4). To evaluate this, we quantified the variance explained by different groups of variables. These groups include Climate (all climate predictors), Topography (latitude, longitude, elevation, and slope), spectral (individual spectral reflectance bands from Landsat composite), and Tasseled Cap (transformed wetness, brightness, and greenness bands). Individually, climate and topography were shown to be the most influential at explaining the variation in the models (7.3 % - 18.7 %), while Landsat-derived products, such as Tassled Cap and individual spectral bands, were less influential (15.0 % - 2.6 %). The combination of topographic predictors, such as elevation and slope, with Landsat spectral data accounted for 75–80 % of the explainable variance across all modeling regions.

Environmental variables that strongly influence vegetation structure influenced structural prediction outcomes in different ways (Fig. 4). For example, with increases in observed elevation, prediction results trended towards lower levels of aboveground biomass. Elevation had the opposite trend for stand age, with stands increasing in age with increasing elevation. Increases in mean annual temperature resulted in increases in aboveground biomass. However, this didn't hold true for stand age, where there seemed to be little effect. Spatial location showed expected patterns of a decreasing ability to support large amounts of aboveground biomass with increasing latitude. Increases in longitude (eastward) also showed an increase in both aboveground biomass and stand age and may be an effect of distance from accessible coastal forest land. A multimodal pattern also emerges when looking at how spatial context affects stand age and biomass, which is likely due to multiple large islands in the region and are also evidence of younger forests being spatially located near coastlines that are easily accessed for the use of timber.

3.2. Forest carbon and structural attribute predictions

Our modeling efforts yielded thirty-nine individual maps of aboveground biomass, forest structure, and composition (e.g., Fig. 6 & 7). The resulting spatial predictions of forest structural attributes showed varying levels of accuracy across the study area. At the plot level, predictions of AGB ($R^2 = 0.38$), stand age ($R^2 = 0.28$), and QMD ($R^2 = 0.36$) demonstrated the highest agreement with observations, while spatial predictions of snag biomass ($R^2 = 0.19$) show the lowest levels of agreement (Fig. 5). The modified leave-one-out cross-validation analysis showed a trend of overpredictions in the lower range of observed values while underpredicting in the upper range (GMFR line). This result is common in Landsat-based approaches to estimating forest structure (Bell et al., 2018). It is also likely attributed to using the mean values across five nearest neighbor maps truncating observed extremes.

Regionally, the distributions of predicted biomass and structural metrics (e.g., Fig. 6) exhibit similar patterns to observed data from field plots. While the predicted median values closely align with the observed values across all plots, the upper and lower quantiles in the predicted values are slightly condensed compared to the observed plot data (Fig. 8). Across all regions, AGB ranged from a median of 5413 $g \cdot m^{-2}$ in Upper Kenai to 38,355 $g \cdot m^{-2}$ in Northern BC, with a total median of 31,506 $g \cdot m^{-2}$. Stand age varied considerably, with the oldest median stands in Southeast Alaska (101 years), while Upper Kenai had the

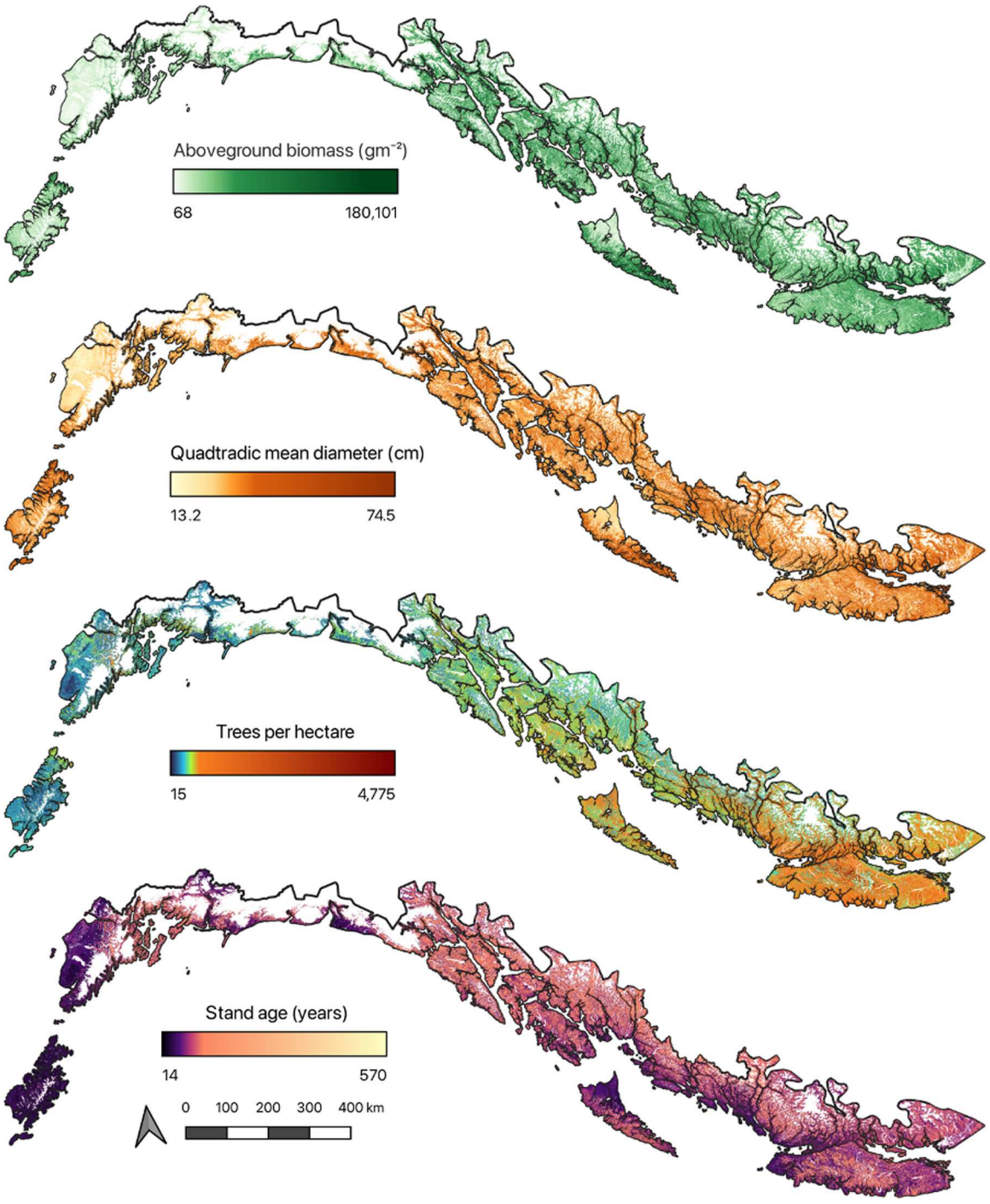

Fig. 6. Mapped results of GNN imputation model for the full modeling region. The four variables selected here represent the main categories of predicted structural metrics.

youngest (50 years). BA and snag biomass showed similar variability, with Southeast Alaska and Northern BC having some of the highest medians. Tree density (TPH) was highest in Southern BC (median 674 trees·hectare^{-1}), and live volume was highest in Northern BC (median 1172 m^3). Across all regions, the total median values for AGB, TPH, and live volume were 31,506 g·m^{-2}, 445 trees·hectare^{-1}, and 1038 m^3, respectively, reflecting substantial variability in forest structure across the study area.

3.3. Imputed maps of individual species

Biomass density maps were created for 19 overstory species in the region (Table 2). These maps provide predictions of species spatial extent and abundance and were compared to mapped plot locations where the species was observed (Fig. 9, A1). The most common species throughout the study area is *Tsuga heterophylla*, with predictions extending throughout the whole mapped region and having a mean live aboveground biomass density of 15,643 g·m^{-2}. While *Chamaecyparis nootkatensis* also had a similar predicted extent, it was less abundant and contributed less overall to the aboveground biomass in the region, with a

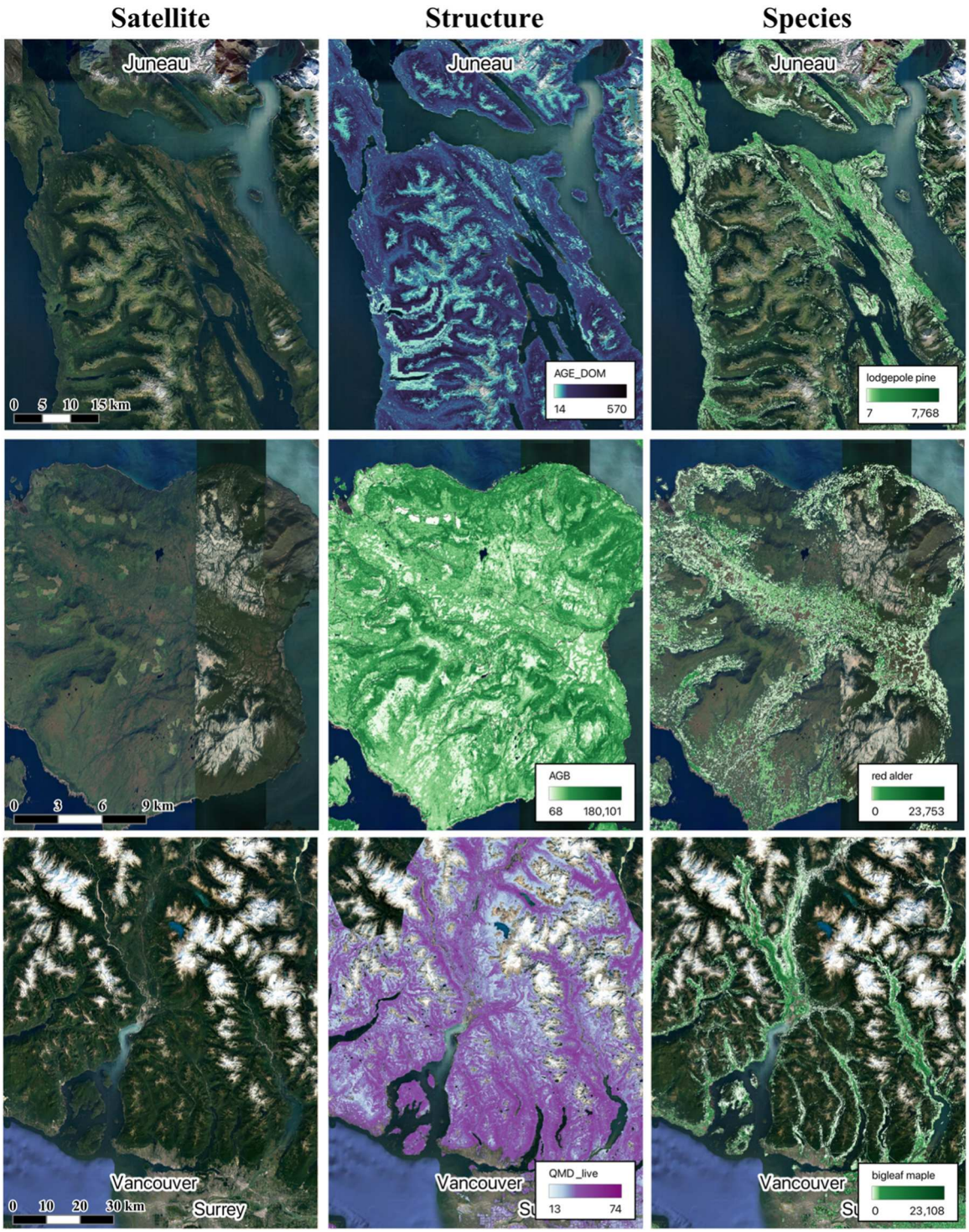

Fig. 7. Examples of forest structural predictions. Rows are representative of different places within the study region, with Juneau on top, Zarembo Island in the middle, and Vancouver on the bottom. Columns represent the satellite imagery, structural attribute, and a select species prediction.

mean live aboveground biomass density of only 5235 $g \cdot m^{-2}$. When comparing the presence of predicted species to the observed plot data, levels of agreement varied significantly by species. We were quite effective at identifying areas where species are not present (low omission error) but were shown to over-predict where species were present, often predicting species presences within their range but not observed at a particular site (high commission error). Commission errors were most substantial in species that have expansive ranges and whose habitat is less constrained to environmental gradients (Table A1), resulting in reduced model performance relative to other species, such as *Picea sitchensis* ($Acc_b = 0.62$) and *Tsuga heterophylla* ($Acc_b = 0.64$), compared to species such as *Pseudotsuga menziesii* ($Acc_b = 0.96$) and *Populus trichocarpa* ($Acc_b = 0.97$). Though broadly distributed, some species with large commission errors have limited spatial extents on the landscapes within relatively broad ranges, such as the presence of *Picea sitchensis* within the western and southern portions of the Kodiak Archipelago and the northern distribution of *Pseudotsuga menziesii* being artificially limited by modeling region.

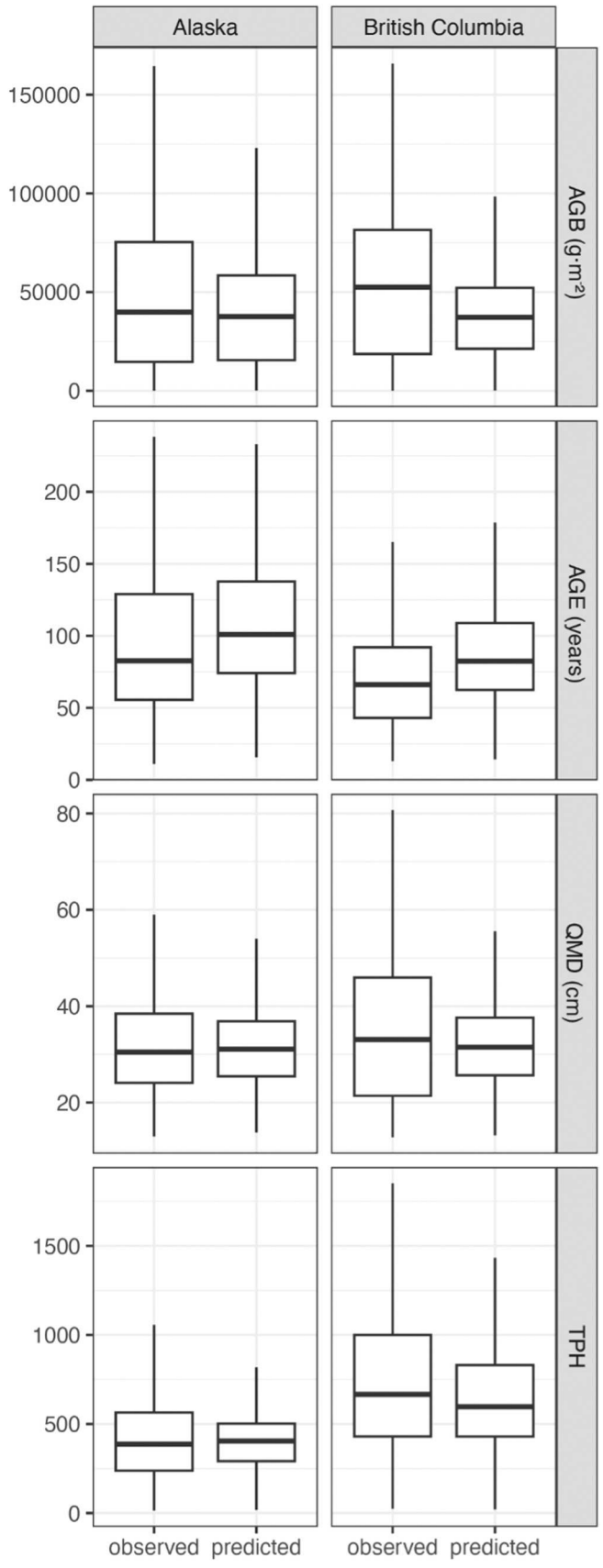

Fig. 8. Comparison of observed (plot data) versus wall-to-wall predicted forest metrics by country.

3.4. Model uncertainty

A map of the mean Euclidian distance in gradient space was made to examine spatial patterns in the uncertainty of our predictions and representation in our training dataset (Fig. 10). The lowest Euclidian distances were seen in low-elevation areas of the Tongass as well as the boreal transition zone of the Kenai, while higher Euclidian distances were observed in areas of high elevation. Patterns of Euclidean distances seemed to be driven by the level of plot support for a particular region, with the lowest Euclidean distances in areas that were well represented by either FIA or FAIB plot data and higher distances in places such as wilderness areas and parks.

4. Discussion

4.1. Predicted patterns across the landscape

4.1.1. Forest biomass and structure

The spatial pattern of forest biomass and structure from the GNN analysis matched expected patterns from observed data and previous publications (Fig. 5; Alaback, 1996; Alaback and Juday, 1989; Harris and Farr, 1974; MacKinnon, 2003). Aboveground biomass was shown to have the highest values at lower elevations; however, this trend becomes less apparent at the lowest elevation nearest to the coastline. This is likely due to the management history in this region, with harvesting targeted in high biomass and low elevation stands that were easy to access (Brackley et al., 2009). Predicted median live aboveground biomass values in the southern modeling regions were lower than those computed from the observed plot data (Fig. 8). This observation may be due to the inclusion of (generally lower biomass) plots from FIA data in Alaska in predictions of forest structure throughout the northern and southern regions of British Columbia. Differences in plot design can introduce artifacts into nearest neighbor imputation, motivating some mapping efforts that avoid mixed plot designs (e.g., Bell et al., 2021). Being that the two forest plot networks work on slightly different data collection protocols, it is difficult to determine if one is underestimating or overestimating forest structural attributes. Because differences in aboveground biomass densities were relatively minor, our integration of these two plot data sources into a GNN may not contribute dramatically to overall errors, but users leveraging the resulting maps across modeling regions should consider the implications for their application.

Although the spatial patterns were similar, our overall predictions of aboveground live biomass in the region trended higher than those of previous studies (Fig. 11). Recent aspatial estimates indicate that the temperate rainforests of Southeast Alaska have an average biomass density of 21,890 $g \cdot m^{-2}$ (Yatskov et al., 2019), which was 44.2 % lower than our estimates of 39,234 $g \cdot m^{-2}$. Global attempts at spatially mapping AGB by Blackard et al., (2008) and Santoro et al., (2018) show that the temperate rainforests of Southeast Alaska have even lower biomass, averaging 19,770 and 14,174 $g \cdot m^{-2}$, respectively. However, our results are in agreement with another recent study (Carter and Buma, 2024), which found that the average AGB was 42,579 $g \cdot m^{-2}$ in the temperate regions of Southeast Alaska and coastal British Columbia, which was only 11 % higher than our estimates of 38,271 $g \cdot m^{-2}$ for the same region. It is important to note that Carter and Buma (2024) also utilized the Kozak taper equations in their biomass estimates. Other sources contributing to higher biomass estimates may include the addition of areas that were not previously accounted for in forest structural estimates, such as wilderness areas and national parks. Additionally, potential bias from pixel saturation observed in optical sensor data may have influenced the estimation of forest biomass (e.g. Lu et al., 2016).

Stand age throughout the region ranged from 14 to 570 years, with Southeast Alaska's having the highest median stand age (101 years). The spatial pattern of stand age was shown to be affected by elevation (Fig. 4), with stand age increasing upslope, likely because they are comprised of longer-lived tree species, such as Alaska yellow cedar. A

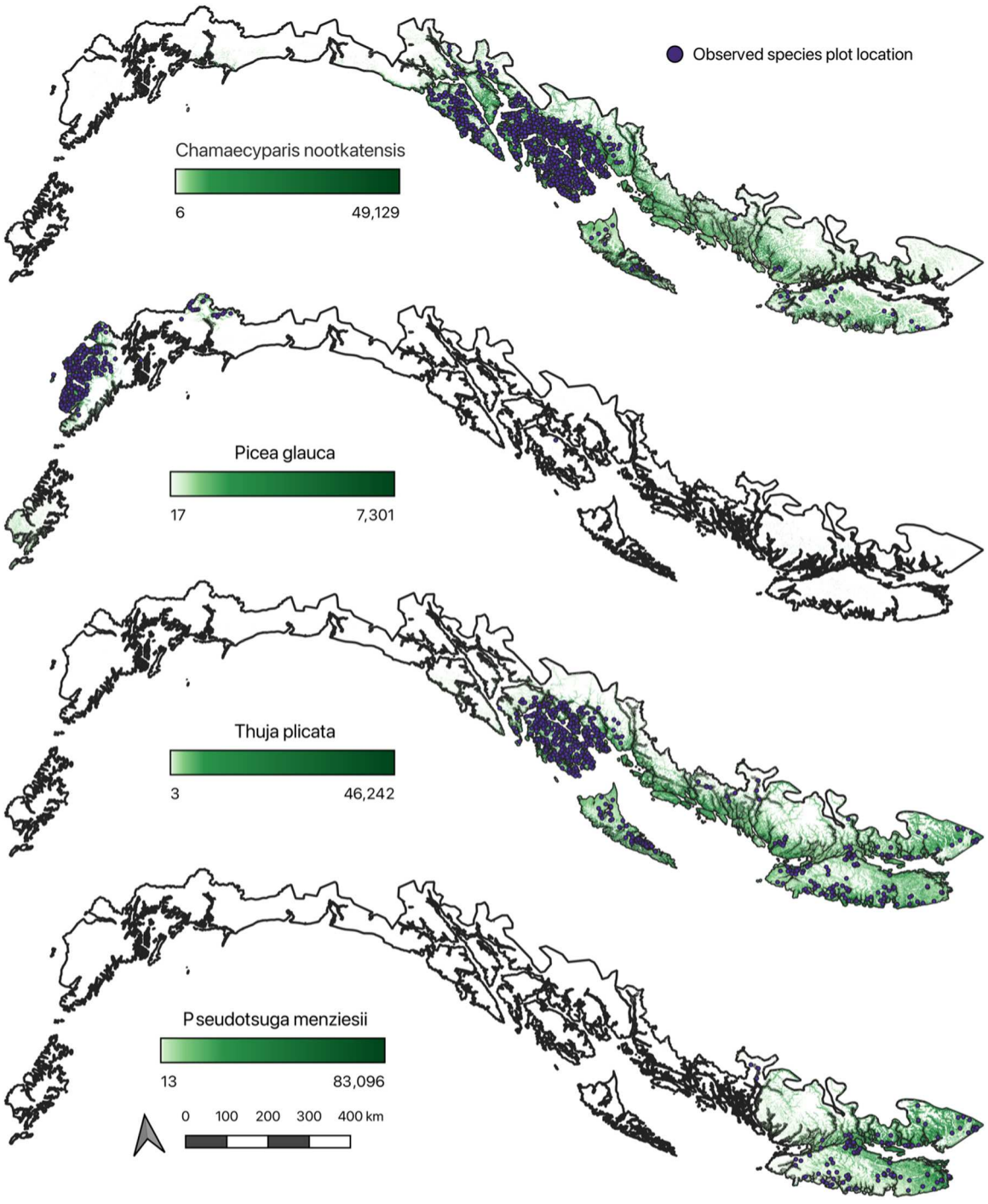

Fig. 9. Mapped results of GNN imputation model for the full modeling region of species biomass (gm^{-2}) and extent. The four species select show the spatial constraints around areas of observed presence. Plot locations shown are the publicly available locations from both FIA and FAIB. Additional species maps can be found in Fig. A1.

sharp drop off in stand age at low elevations near the coast may also be a combination of shorter-lived species, such as red alder, and previous harvest activities targeted towards low-lying and easily accessible stands. Although younger, forests in British Columbia were shown to have larger trees (higher median QMD), and denser forests (higher TPH), likely attributing to similar aboveground biomass densities compared to forests in Southeast Alaska (Table 5, Fig. 8).

4.1.2. Individual species predictions

Despite the relatively good agreement between predicted and observed data (Fig. 5), there was a tendency toward commission errors (Table A1), with individual species being predicted within their known range (Fryer, 2018) but within plots where their presence was not actually observed. This issue has been noted in other studies using similar methods to estimate forest structural attributes in the Pacific Northwest (Irvine, 2022; Ohmann and Gregory, 2002). These errors likely stem from using the mean value from the five nearest neighbors and the reliance on spectral and climate data as predictors. Much like climate envelope modeling, commission errors can result from environmental factors indicating suitable conditions for a species without

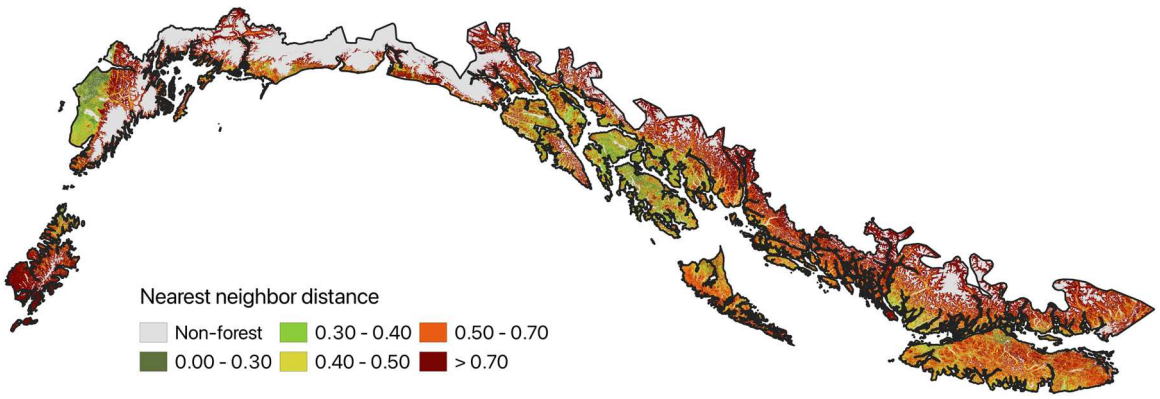

Fig. 10. Map of mean nearest-neighbor distances for the k = 5 nearest neighbor predictions. Values in this map represent the mean Euclidean distance from the environmental gradients a pixel represents to the nearest-neighbor imputed by GNN.

accounting for limitations such as seed availability or geographic barriers (Elith and Leathwick, 2009). In this study, we addressed these issues by creating separate modeling regions based on environmental and vegetative conditions and the inclusion of spatial location as a predictor variable. Despite these measures, these uncertainties should be considered when using these predictions.

4.2. Regional challenges

The amount of uncertainty in forest predictions varied by region, as seen in Fig. 10. Areas with higher levels of uncertainty (i.e., greater Euclidian distances) can be attributed to various sources, such as the vicinity and density of plot data to a prediction cell, the quality of the spectral data used, how parsimonious the model used may be, and uncertainties in datasets chosen as predictors. Below, we discuss those topics in relation to the temperate rainforests of North America.

4.2.1. Scarcity of plot data

The FIA program in the United States and British Columbias FAIB are both government-led initiatives tasked with monitoring and assessing the status and trends of their respective countries' forest resources. Both programs have comprehensive approaches to forest inventory, collecting data on forest extent, composition, and health, and play crucial roles in providing valuable information to support informed decision-making, policy development, and sustainable forest management practices. However, there are notable differences between the two programs. One significant distinction is the availability of plot data, particularly in coastal British Columbia (Fig. 2). While the FIA program in the United States maintains a robust network of permanent sample plots across all forested regions (with the exception of Glacier Bay National Park and wilderness areas), the FAIB dataset in British Columbia lacks spatial coverage of the northern portions of the British Columbia coast. This data gap poses challenges for accurately assessing forest conditions and trends in this ecologically diverse and economically significant region, whether using plot-based estimation approaches or model-based approaches (e.g., GNN).

Furthermore, FAIB employs both fixed and variable radius plots; variable radius plots allow for flexible plot sizes based on tree diameter (Avery and Burkhart, 1983), whereas FIA annual plot design uses a series of fixed radius plots at each survey site (Gray et al., 2012). Previous studies show that the FIA fixed-radius plot design may lead to an underestimation of tree density and volume in stands with large, spaced out trees (Gray, 2003), while variable radius plots may be biased towards trees with higher basal areas (Azuma and Monleon, 2011), and lead to potentially overestimated stand volume. This difference in sampling methodology can present challenges when making regional estimates of forest structure, particularly when those estimates cross political boundaries. Due to the differences in methodologies and resulting plot-level estimates between fixed and variable radius plots, all variable radius plots included in FAIB were omitted and only fixed area plots were used. This also had the effect of further diminishing the plot densities in the southern region of the study area.

4.2.2. Quality of Landsat mosaic

Obtaining a complete Landsat mosaic in the temperate rainforests of North America poses significant challenges due to environmental conditions inherent to these regions. High latitudes, characteristic of temperate rainforests, often result in terrain shadows, particularly in areas with rugged topography, such as coastal mountains (Giles, 2001). These shadows can obscure large portions of the landscape from satellite sensors, leading to incomplete coverage in Landsat imagery (Schulmann et al., 2015) or to overestimation of forest biomass and stand age as models may confuse terrain shadowing with increased shadowing related to tall, structurally complex forests (Irvine, 2022). Additionally, consistent cloud cover and snowfall further complicate the acquisition of high-quality satellite data (Braaten et al., 2015). Complete cloud cover is frequent over the skies of the temperate rainforests, obstructing the view of the Earth's surface and limiting the availability of cloud-free imagery for mosaic creation. Similarly, snow cover, which can persist for extended periods in these regions, adds another layer of complexity by altering surface reflectance properties and reducing the visibility of underlying features.

In addition, obtaining remotely sensed imagery over a site within a relatively close timeframe to the observed plot data collection is difficult. Developing methods that better allowed for temporal matches between observed plot data collection and remotely sensed reflectance values could improve overall model predictions (e.g., McRoberts et al., 2016).

4.2.3. Downscaled climate variables

Using downscaled CMIP5 global climate model data, particularly in regions characterized by high topographic variability, can introduce significant uncertainties into climate projections (Foley, 2010; Wootten et al., 2017). Global climate models typically have coarse spatial resolutions, which may not adequately capture local-scale variations in terrain, land cover, and atmospheric dynamics. When downscaling these coarse-resolution climate model outputs to finer spatial scales, such as those relevant for regional or local climate assessments, uncertainties can arise due to the inability of downscaling methods to accurately represent complex topographic features (Ahmadalipour et al., 2018). In areas with high topographic variability, such as the mountainous regions of the coastal temperate rainforest, even downscaled climate projections may struggle to capture the intricate interactions between elevation, slope, aspect, and microclimatic conditions. Additionally, the choice of downscaling technique, the resolution of input data, and the treatment of physical processes can further contribute to uncertainties in

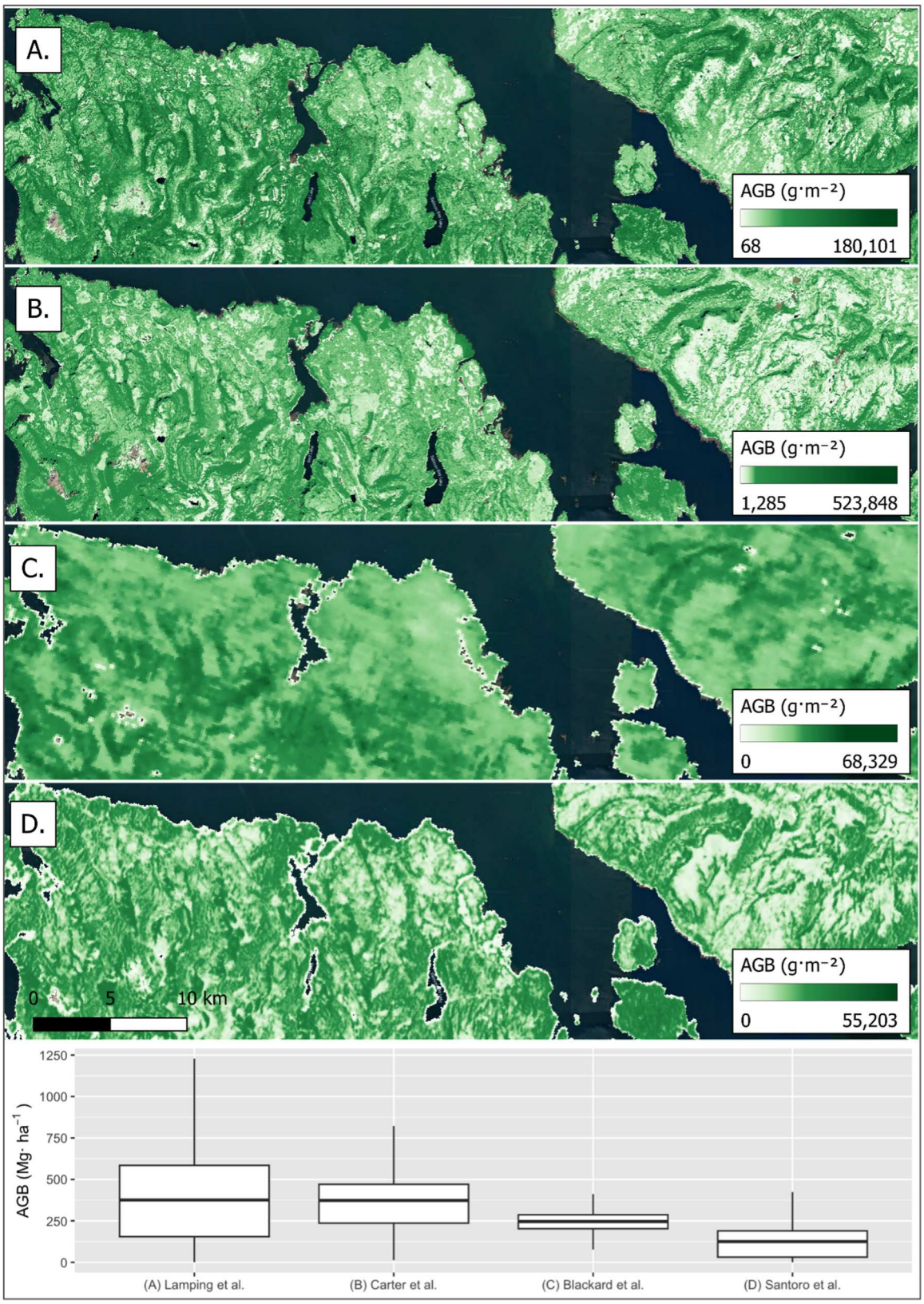

Fig. 11. Comparison between the GNN aboveground biomass results of this study to other regional and global studies for the Tongass National Forest. Lowermost panel compares the distribution of living aboveground biomass ($Mg{\cdot}ha^{-1}$, outliers omitted) between that of other studies with their corresponding maps above. Studies include A. this study (30 m), B. Carter and Buma (2024) (30 m), C. Blackard et al. (2008) (250 m), and D. Santoro et al. (2018) (100 m).

Table 5
Mean values of imputed GNN structural data for AGB, stand age, BA, snag biomass, TPH, and live volume. Means are shown for each modeling region.

	Variable	Unit	Mean
Upper Kenai	AGB	$g \cdot m^{-2}$	6773
	Stand age	years	51
	BA	$cm^2 \cdot h^{-1}$	8
	Snag biomass	$g \cdot m^{-2}$	1982
	TPH	$trees \cdot hectare^{-1}$	230
	Live volume	m^3	170
Gulf of AK	AGB	$g \cdot m^{-2}$	18,874
	Stand age	years	73
	BA	$cm^2 \cdot h^{-1}$	20
	Snag biomass	$g \cdot m^{-2}$	1584
	TPH	$trees \cdot hectare^{-1}$	278
	Live volume	m^3	484
Southeast AK	AGB	$g \cdot m^{-2}$	39,234
	Stand age	years	113
	BA	$cm^2 \cdot h^{-1}$	33
	Snag biomass	$g \cdot m^{-2}$	6791
	TPH	$trees \cdot hectare^{-1}$	396
	Live volume	m^3	978
Northern BC	AGB	$g \cdot m^{-2}$	38,440
	Stand age	years	98
	BA	$cm^2 \cdot h^{-1}$	43
	Snag biomass	$g \cdot m^{-2}$	531
	TPH	$trees \cdot hectare^{-1}$	720
	Live volume	m^3	1438
Southern BC	AGB	$g \cdot m^{-2}$	37,235
	Stand age	years	91
	BA	$cm^2 \cdot h^{-1}$	53
	Snag biomass	$g \cdot m^{-2}$	6536
	TPH	$trees \cdot hectare^{-1}$	820
	Live volume	m^3	3139
Total	AGB	$g \cdot m^{-2}$	33,726
	Stand age	years	94
	BA	$cm^2 \cdot h^{-1}$	38
	Snag biomass	$g \cdot m^{-2}$	5544
	TPH	$trees \cdot hectare^{-1}$	525
	Live volume	m^3	1619

downscaled climate projections. Therefore, careful consideration of these factors should be taken into account when choosing to use downscaled climate variables as predictors in GNN, particularly in regions with pronounced topographic variability.

4.2.4. Predictor selection

Canonical correspondence analysis (CCA) offers a robust alternative to multiple linear regression, particularly for handling data with numerous null values and non-normal distributions (Ter Braak, 1986). Unlike multiple linear regression, CCA does not require iterative successional runs to understand the effects of multiple predictors on numerous response variables. However, the careful selection of predictor variables remains crucial for effective model development and to avoid the issues associated with overly complex models (Bell and Schlaepfer, 2016). Previous studies in the Pacific Northwest found that using individual spectral bands from Landsat decreased model performance (Ohmann et al., 2007; Ohmann and Gregory, 2002). This can be different depending on forest conditions and reflectance values and, for this study, exploratory attempts showed higher agreement in prediction outcomes with all Landsat 8 bands included in the CCA. In the final model, the individual Landsat bands showed little explanatory power, while the various spectral indices showed stronger relations in predicting forest structure (Fig. 3). Choosing appropriate environmental predictors is essential, as community assemblages or structural conditions often correlate with similar environmental factors across the landscape.

4.3. Management applications

Our spatially comprehensive maps, which extend from Kodiak Island down to the southern border of British Columbia, offer valuable opportunities to inform research, management, or policy decisions. For instance, this dataset enables consistent carbon accounting across the North American temperate rainforest, supporting climate change mitigation strategies under international agreements. It can also guide cross-border conservation planning by identifying high-biomass or structurally unique areas, inform wildfire risk management by highlighting vulnerable forest structures, and support biodiversity initiatives by identifying critical habitats for species with ranges spanning the Canada–US border. Similar vegetation maps in other regions have been utilized to assess regional biomass and carbon storage, monitor disturbance patterns, track land cover changes over time, and study vegetation responses to climatic shifts (Carter and Buma, 2024; Griesbauer and Scott Green, 2010; McNicol et al., 2019; Nowacki and Kramer, 1998). In the temperate forests of Southeast and southcentral Alaska and coastal British Columbia, these data can facilitate research on carbon and nutrient fluxes, investigate spatial patterns of forest structural classes critical for wildlife habitats, as well as informing regional forest landscape models of initial vegetative conditions.

5. Conclusion

Ecosystems in coastal Alaska and British Columbia are significant carbon reservoirs, storing approximately 3.58 Pg of terrestrial carbon. Although generally thought to be buffered by the coastal climate, climate change projections suggest complex responses in these ecosystems, with potential increases in carbon emissions in the boreal region, increases in sequestration rates in the coastal temperate zone, and changes in the balance of precipitation that falls as snow (Shanley et al., 2015). Although timber harvest in this region has declined, it still remains actively managed in support of local and global economies, and significantly impacts carbon storage and ecosystem services (Crotteau et al., 2022). Regardless, Southeast Alaska and coastal British Columbia comprise a significant portion of the Earth's remaining old-growth temperate rainforest, primarily held within Inventoried Roadless Areas (IRAs), Wilderness, and old growth reserves. However, changes in management priorities within IRAs present potential changes to these ecosystems and necessitate more comprehensive information about the forests in these areas, particularly given the recent shifts in regional forest management that focus on young growth harvesting, conservation of old growth, and carbon sequestration (DellaSala et al., 2022; Law et al., 2023).

Our 30-m resolution maps of aboveground biomass, forest structure, and species composition extend across the entire coastal regions of southern Alaska and British Columbia, traversing political boundaries, land ownerships, administrative jurisdictions, and ecological gradients. These spatially-complete maps may help land managers assess spatial patterns of forest structural attributes and be used in assessments of timber supply, carbon stocks, and delineation of potential wildlife habitat. They may also form the foundation for modeling efforts to assess the climate vulnerability of this vast C-rich ecosystem.

CRediT authorship contribution statement

Lucash Melissa: Writing – review & editing, Supervision, Project administration, Funding acquisition. **Lamping James Edward:** Writing – original draft, Validation, Formal analysis, Data curation, Conceptualization. **Gregory Matt:** Writing – review & editing, Methodology. **Irvine Daniel R.:** Writing – review & editing, Methodology, Data curation. **Bell David M.:** Writing – review & editing, Methodology, Data curation.

Declaration of Competing Interest

The authors declare that they have no known competing financial interests or personal relationships that could have appeared to influence the work reported in this paper.

Acknowledgements

Thank you to Harold Zald and Dave D'Amore at the USDA Forest Service, as well as Caren Dymond and Sari Saunders at the British Columbia Ministry of Forests for their technical and regional insights. Also, thank you to Brian Buma (the PI of the grant for which this research was funded) and Trevor Carter for their continuous feedback and data sharing. This work was supported by the National Science Foundation award #: 2025726 and the USDA Forest Service Pacific Northwest Research Station (19-JV-11261959–064, 22-JV-11261959–067).

Appendix

Table A1
Species specific accuracy (Acc), balanced accuracy (Acc_b), omission, and commission error

Species	Acc	Acc_b	Omission Error	Commission Error
Abies amabilis	0.941	0.970	0.000	0.788
Abies lasiocarpa	0.989	0.994	0.000	0.968
Alnus rubra	0.794	0.883	0.043	0.863
Betula papyrifera	0.888	0.942	0.015	0.824
Chamaecyparis nootkatensis	0.615	0.790	0.005	0.842
Picea glauca	0.931	0.964	0.021	0.575
Picea mariana	0.953	0.976	0.018	0.700
Picea sitchensis	0.365	0.618	0.022	0.791
Pinus contorta	0.752	0.872	0.011	0.877
Populus tremuloides	0.947	0.974	0.200	0.947
Populus trichocarpa	0.901	0.942	0.028	0.793
Pseudotsuga menziesii	0.915	0.956	0.000	0.774
Taxus brevifolia	0.984	0.992	0.000	0.978
Thuja plicata	0.631	0.804	0.019	0.864
Tsuga heterophylla	0.505	0.644	0.026	0.620
Tsuga mertensiana	0.567	0.741	0.014	0.729

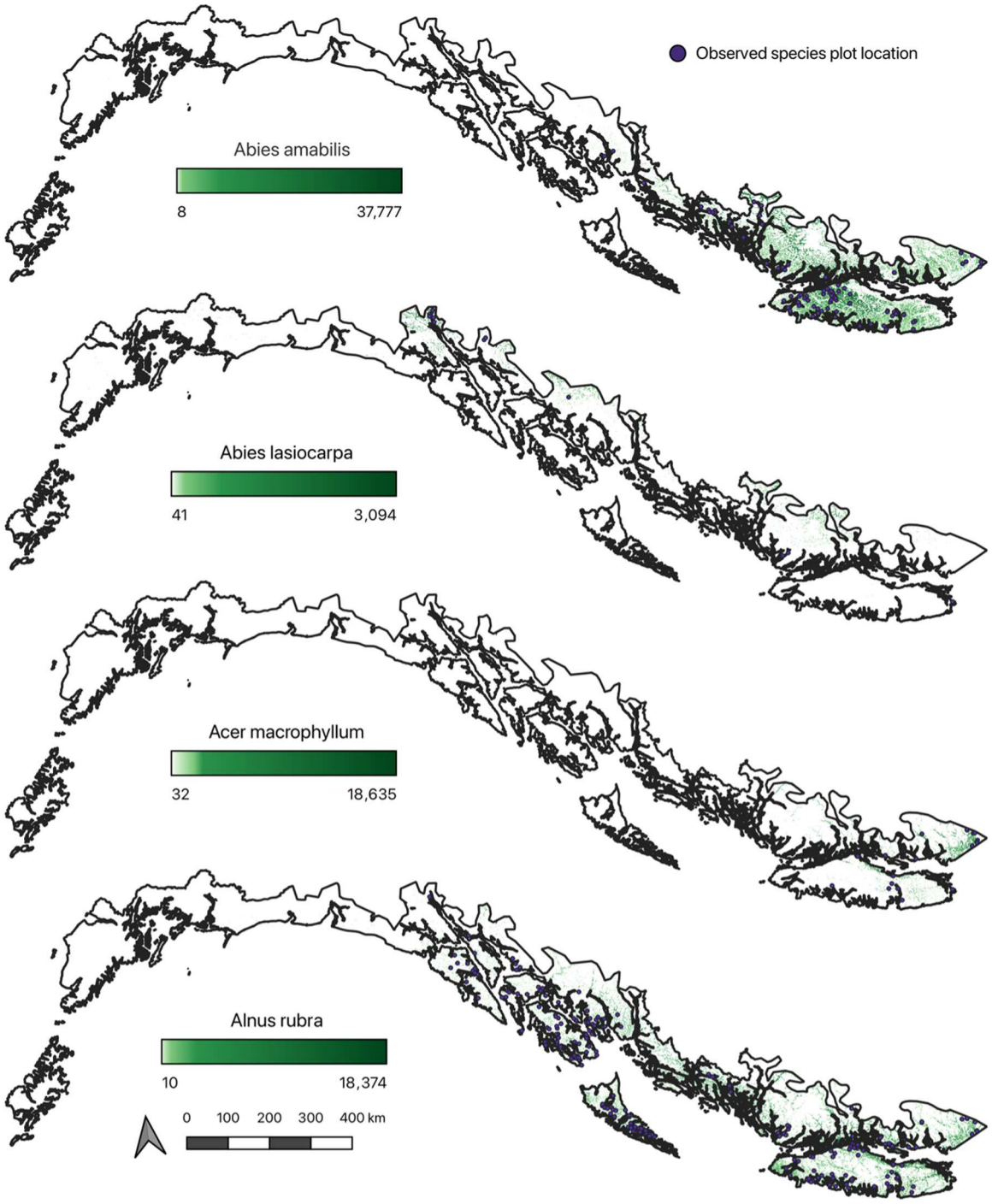

Figure A1A. Mapped results of GNN imputation model for the full modeling region of species biomass (gm^{-2}) and extent. The four species select show the spatial constraints around areas of observed presence. Plot locations shown are the publicly available locations from both FIA and FAIB

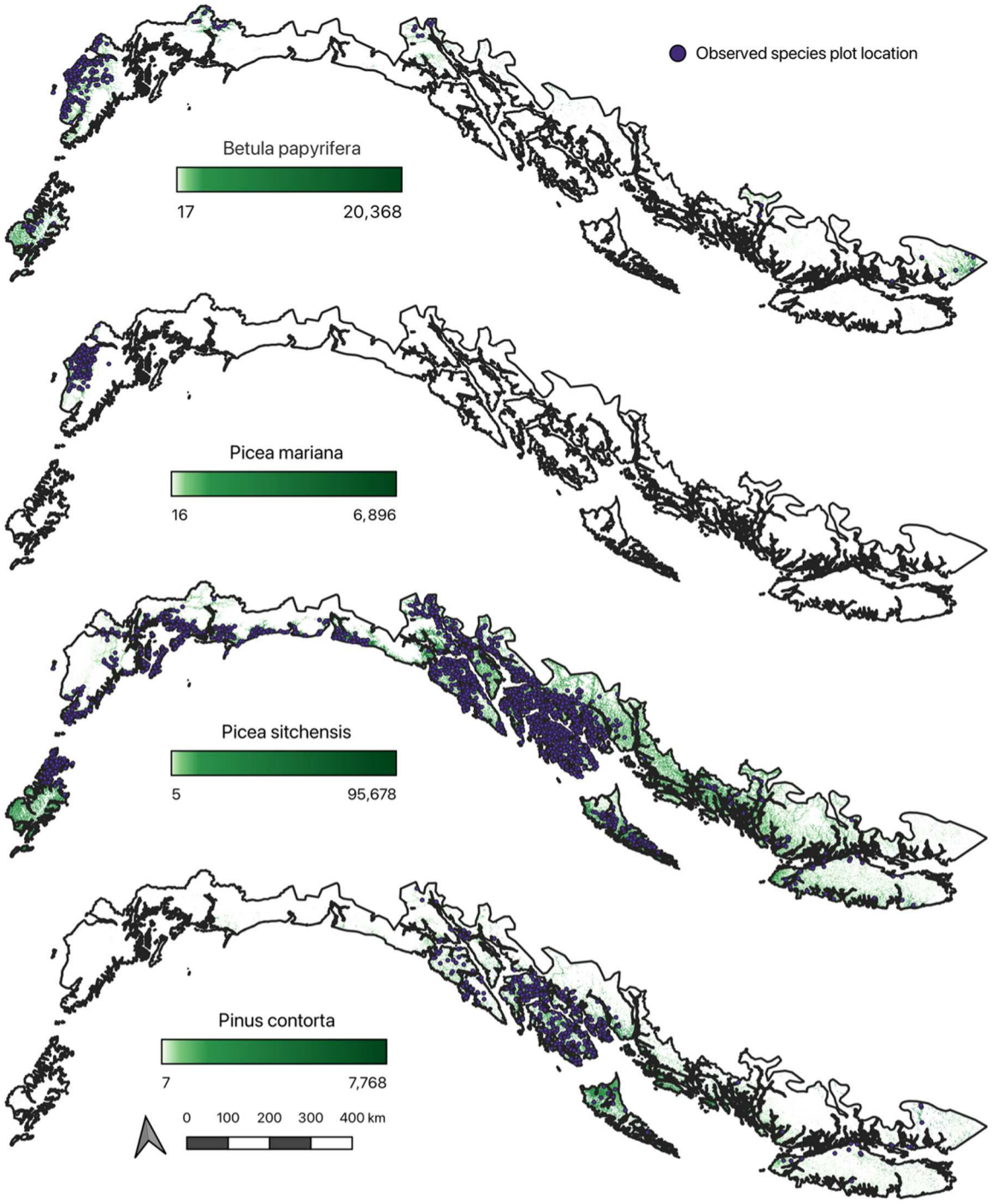

Figure A1B. Mapped results of GNN imputation model for the full modeling region of species biomass (gm^{-2}) and extent. The four species select show the spatial constraints around areas of observed presence. Plot locations shown are the publicly available locations from both FIA and FAIB

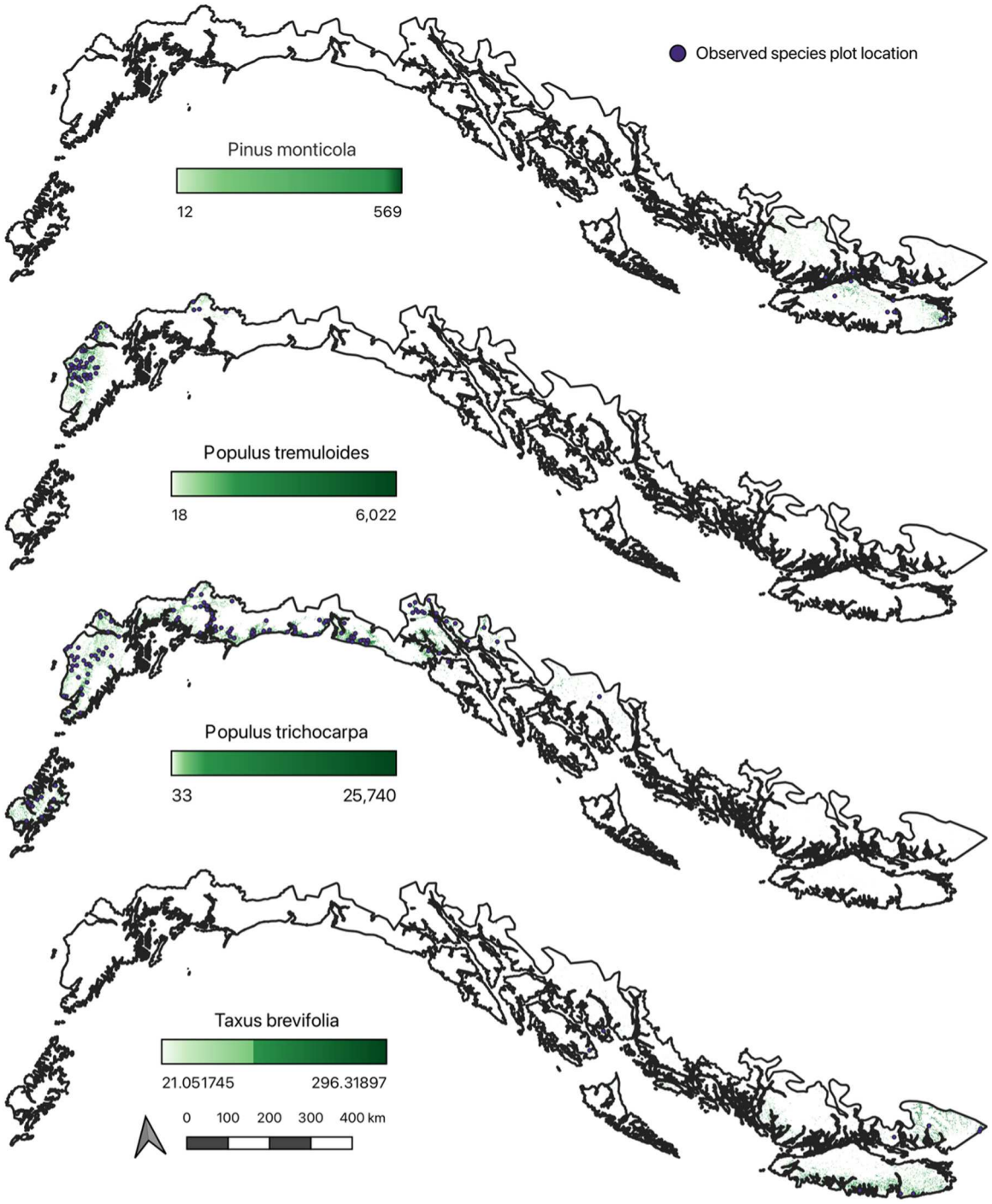

Figure A1C. Mapped results of GNN imputation model for the full modeling region of species biomass (gm^{-2}) and extent. The four species select show the spatial constraints around areas of observed presence. Plot locations shown are the publicly available locations from both FIA and FAIB

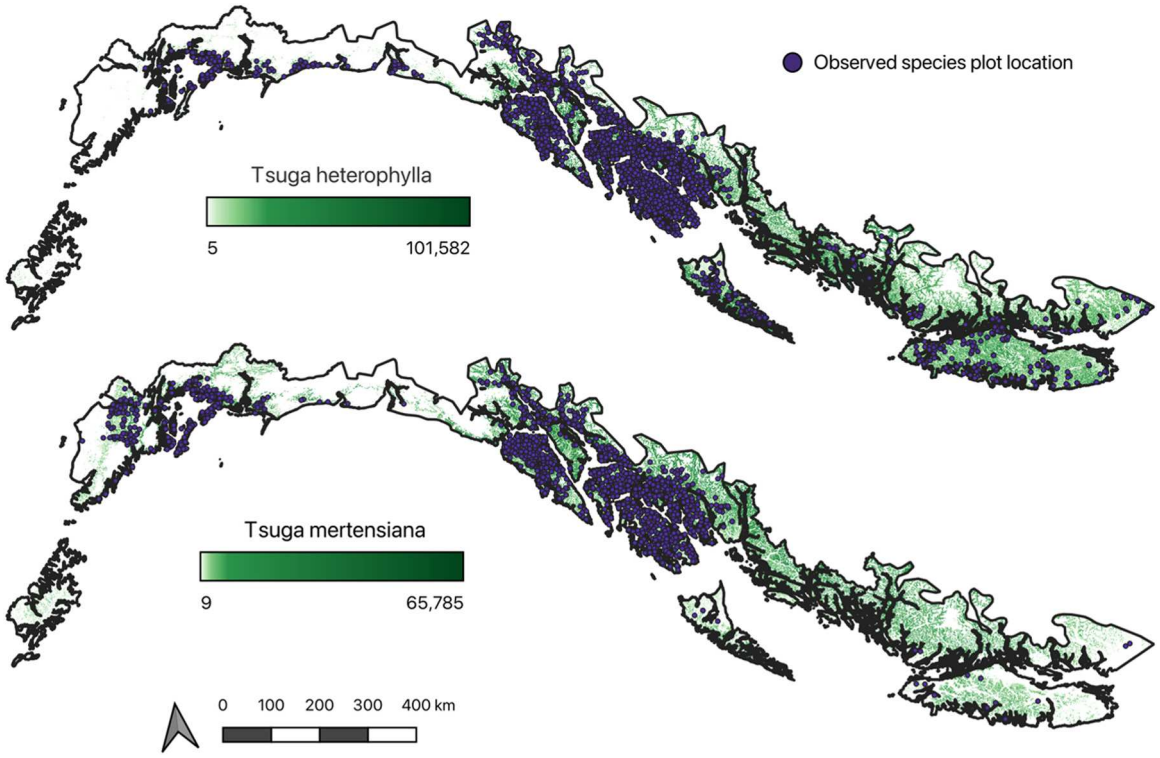

Figure A1D. Mapped results of GNN imputation model for the full modeling region of species biomass (gm^{-2}) and extent. The four species select show the spatial constraints around areas of observed presence. Plot locations shown are the publicly available locations from both FIA and FAIB

Data availability

Maps generated from this study can be found at https://doi.org/10.5281/zenodo.13932139. Underlying forest plot data is confidential and cannot be shared. Publically available "fuzzed" plot data and code can be requested.

References

Ahmadalipour, A., Moradkhani, H., Rana, A., 2018. Accounting for downscaling and model uncertainty in fine-resolution seasonal climate projections over the Columbia River Basin. Clim. Dyn. 50, 717–733. https://doi.org/10.1007/s00382-017-3639-4.

Alaback, P.B., 1996. Biodiversity Patterns in Relation to Climate: The Coastal Temperate Rainforests of North America. In: Lawford, R.G., Fuentes, E., Alaback, P.B. (Eds.), High-Latitude Rainforests and Associated Ecosystems of the West Coast of the Americas, Ecological Studies. Springer New York, New York, NY, pp. 105–133. https://doi.org/10.1007/978-1-4612-3970-3_7.

Alaback, P.B., Juday, G.P., 1989. Structure and composition of low elevation old-growth forests in research natural areas of Southeast Alaska. Nat. Areas J. 9, 27–39.

Avery, T.E., Burkhart, H.E., 1983. Forest measurements. McGraw-Hill Book Company.

Azuma, D., Monleon, V.J., 2011. Differences in forest area classification based on tree tally from variable- and fixed-radius plots. Can. J. For. Res. 41, 211–214. https://doi.org/10.1139/x10-200.

Banskota, A., Kayastha, N., Falkowski, M.J., Wulder, M.A., Froese, R.E., White, J.C., 2014. Forest monitoring using landsat time series data: a review. Can. J. Remote Sens. 40, 362–384. https://doi.org/10.1080/07038992.2014.987376.

Beamish, A., Raynolds, M.K., Epstein, H., Frost, G.V., Macander, M.J., Bergstedt, H., Bartsch, A., Kruse, S., Miles, V., Tanis, C.M., 2020. Recent trends and remaining challenges for optical remote sensing of Arctic tundra vegetation: a review and outlook. Remote Sens. Environ. 246, 111872.

Bell, D.M., Acker, S.A., Gregory, M.J., Davis, R.J., Garcia, B.A., 2021. Quantifying regional trends in large live tree and snag availability in support of forest management. For. Ecol. Manag. 479, 118554.

Bell, D.M., Gregory, M.J., Kane, V., Kane, J., Kennedy, R.E., Roberts, H.M., Yang, Z., 2018. Multiscale divergence between Landsat- and lidar-based biomass mapping is related to regional variation in canopy cover and composition. Carbon Balance Manag. 13, 15. https://doi.org/10.1186/s13021-018-0104-6.

Bell, D.M., Gregory, M.J., Palmer, M., Davis, R., 2023. Guidance for forest management and landscape ecology applications of recent gradient nearest neighbor imputation maps in California, Oregon, and Washington. In: Gen. Tech. Rep. PNW-GTR-1018, 41. U.S. Department of Agriculture, Forest Service, Pacific Northwest Research Station, Portland, OR, p. 1018. https://doi.org/10.2737/PNW-GTR-1018 (Online only).

Bell, D.M., Schlaepfer, D.R., 2016. On the dangers of model complexity without ecological justification in species distribution modeling. Ecol. Model. 330, 50–59.

Berner, L.T., Jantz, P., Tape, K.D., Goetz, S.J., 2018. Tundra plant above-ground biomass and shrub dominance mapped across the North Slope of Alaska. Environ. Res. Lett. 13, 035002.

Bidlack, A., Bisbing, S., Buma, B., D'Amore, D., Hennon, P., Heutte, T., Krapek, J., Mulvey, R., Oakes, L., 2017. Alternative interpretation and scale-based context for "No evidence of recent (1995–2013) decrease of yellow-cedar in Alaska" (Barrett and Pattison 2017). Can. J. For. Res. 47, 1145–1151. https://doi.org/10.1139/cjfr-2017-0070.

Blackard, J.A., Finco, M.V., Helmer, E.H., Holden, G.R., Hoppus, M.L., Jacobs, D.M., Lister, A.J., Moisen, G.G., Nelson, M.D., Riemann, R., 2008. Mapping US forest biomass using nationwide forest inventory data and moderate resolution information. Remote Sens. Environ. 112, 1658–1677.

Braaten, J.D., Cohen, W.B., Yang, Z., 2015. Automated cloud and cloud shadow identification in Landsat MSS imagery for temperate ecosystems. Remote Sens. Environ. 169, 128–138. https://doi.org/10.1016/j.rse.2015.08.006.

Brackley, A.M., Haynes, R.W., Alexander, S.J., 2009. Timber harvests in Alaska: 1910-2006 (No. PNW-RN-560). U.S. Department of Agriculture, Forest Service, Pacific Northwest Research Station, Portland, OR. https://doi.org/10.2737/PNW-RN-560.

Buma, B., Krapek, J., Edwards, R.T., 2016. Watershed-scale forest biomass distribution in a perhumid temperate rainforest as driven by topographic, soil, and disturbance variables. Can. J. For. Res. 46, 844–854. https://doi.org/10.1139/cjfr-2016-0041.

Carter, T.A., Buma, B., 2024. The Distribution of Tree Biomass Carbon within the Pacific Coastal Temperate Rainforest, a Disproportionally Carbon Dense Forest. Can. J. For. Res. cjfr-2024-0015. https://doi.org/10.1139/cjfr-2024-0015.

Chirici, G., Mura, M., McInerney, D., Py, N., Tomppo, E.O., Waser, L.T., Travaglini, D., McRoberts, R.E., 2016. A meta-analysis and review of the literature on the k-Nearest Neighbors technique for forestry applications that use remotely sensed data. Remote Sens. Environ. 176, 282–294. https://doi.org/10.1016/j.rse.2016.02.001.

Chojnacky, D.C., Heath, L.S., Jenkins, J.C., 2014. Updated generalized biomass equations for North American tree species. Forestry 87, 129–151. https://doi.org/10.1093/forestry/cpt053.

Cohen, W.B., Goward, S.N., 2004. Landsat's role in ecological applications of remote sensing. BioScience 54, 535–545. https://doi.org/10.1641/0006-3568(2004)054[0535:LRIEAO]2.0.CO;2.

Crist, E.P., Cicone, R.C., 1984. A physically-based transformation of Thematic Mapper data—The TM Tasseled Cap. IEEE Trans. Geosci. Remote Sens. 256, 263.

Crone, L.K., Mehrkens, J.R., 2013. Indigenous and commercial uses of the natural resources of the north pacific rainforest with a focus on southeast Alaska and Haida Gwaii. in: North Pacific Temperate Rainforests: Ecology and Conservation. University of Washington Press Seattle, pp. 89–126.

Crotteau, J.S., D'amore, D.V., Barnard, J.C., Lawton, G., Mcfarland, J., 2022. Commercial thinning strategies in southeast Alaska: establishment and effects of the Prince of Wales Commercial Thinning Study. Gen. Tech. Rep. PNW-GTR-1012. Portland, OR: U. S. Dep. Agric., For. Serv., Pac. Northwest Res. Station 77. https://doi.org/10.2737/PNW-GTR-1012.

DeGayner, E.J., Kramer, M.G., Doerr, J.G., Robertsen, M.J., 2005. Windstorm disturbance effects on forest structure and Black Bear Dens in Southeast Alaska. Ecol. Appl. 15, 1306–1316. https://doi.org/10.1890/03-5385.

DellaSala, D.A., Gorelik, S.R., Walker, W.S., 2022. The Tongass National Forest, Southeast Alaska, USA: A Natural Climate Solution of Global Significance. Land 11, 717. https://doi.org/10.3390/land11050717.

DellaSala, D.A., Moola, F., Alaback, P., Paquet, P.C., Schoen, J.W., Noss, R.F., 2011. Temperate and Boreal Rainforests of the Pacific Coast of North America. In: DellaSala, D.A. (Ed.), Temperate and Boreal Rainforests of the World: Ecology and Conservation. Island Press/Center for Resource Economics, Washington, DC, pp. 42–81. https://doi.org/10.5822/978-1-61091-008-8_2.

Elith, J., Leathwick, J.R., 2009. Species distribution models: ecological explanation and prediction across space and time. Annu. Rev. Ecol. Evol. Syst. 40, 677–697. https://doi.org/10.1146/annurev.ecolsys.110308.120159.

Fassnacht, F.E., White, J.C., Wulder, M.A., Næsset, E., 2024. Remote sensing in forestry: current challenges, considerations and directions. For.: Int. J. For. Res. 97, 11–37. https://doi.org/10.1093/forestry/cpad024.

Foley, A.M., 2010. Uncertainty in regional climate modelling: a review. Prog. Phys. Geogr.: Earth Environ. 34, 647–670. https://doi.org/10.1177/0309133310375654.

Forest Analysis and Inventory Branch, 2023. B.C. Timber Harvest Boundaries.

Fryer, J., 2018. Tree species distribution maps from Little's "Atlas of United States trees" series. [WWW Document]. Fire Effects Information System. URL ⟨https://www.fs.usda.gov/database/feis/pdfs/Little/aa_SupportingFiles/LittleMaps.html⟩.

Giles, P.T., 2001. Remote sensing and cast shadows in mountainous terrain. Photogramm. Eng. Remote Sens. 67, 833–840.

Gorelick, N., Hancher, M., Dixon, M., Ilyushchenko, S., Thau, D., Moore, R., 2017. Google Earth Engine: Planetary-scale geospatial analysis for everyone. Remote Sensing of Environment. https://doi.org/10.1016/j.rse.2017.06.031.

Government of British Columbia, 2023. Forest Inventory Ground Plot Data and Interactive Map - Open Government Portal.

Gray, A., 2003. Monitoring stand structure in mature coastal Douglas-®r forests: effect of plot size. Forest Ecology and Management.

Gray, A.N., Brandeis, T.J., Shaw, J.D., McWilliams, W.H., Miles, P.D., 2012. Forest inventory and analysis database of the United States of America (FIA). Biodiversity, Evolution and Ecology of Plants.

Griesbauer, H.P., Scott Green, D., 2010. Assessing the climatic sensitivity of Douglas-fir at its northern range margins in British Columbia, Canada. Trees 24, 375–389. https://doi.org/10.1007/s00468-009-0407-z.

Harris, A., Farr, W., 1974. The forest ecosystem of southeast Alaska (No. PNW-25). USDA Forest Service, Pacific Northwest Research Station.

Hermann, R.K., Lavender, D.P., 1990. Pseudotsuga menziesii (Mirb.) franco Douglas-fir. Silvics of North America 1.

Hermosilla, T., Bastyr, A., Coops, N.C., White, J.C., Wulder, M.A., 2022. Mapping the presence and distribution of tree species in Canada's forested ecosystems. Remote Sens. Environ. 282, 113276. https://doi.org/10.1016/j.rse.2022.113276.

Hijmans, R.J., 2023. terra: Spatial Data Analysis.

Hurni, K., Heinimann, A., Würsch, L., 2017. Google earth engine image pre-processing tool: background and methods.

Irvine, D., 2022. Wall-to-Wall Forest Mapping in Southeast and Southcentral Alaska: A New Application of the Gradient Nearest Neighbor Approach. Oregon State University.

Jenkins, J.C., Chojnacky, D.C., Heath, L.S., Birdsey, R.A., 2003. National-scale biomass estimators for United States tree species. For. Sci. 49, 12–35. https://doi.org/10.1093/forestscience/49.1.12.

Kane, V.R., Gillespie, A.R., McGaughey, R., Lutz, J.A., Ceder, K., Franklin, J.F., 2008. Interpretation and topographic compensation of conifer canopy self-shadowing. Remote Sens. Environ. 112, 3820–3832.

Karger, D.N., Conrad, O., Böhner, J., Kawohl, T., Kreft, H., Soria-Auza, R.W., Zimmermann, N.E., Linder, H.P., Kessler, M., 2017. Climatologies at high resolution for the earth's land surface areas. Sci. Data 4, 170122. https://doi.org/10.1038/sdata.2017.122.

Kennedy, R.E., Andréfouët, S., Cohen, W.B., Gómez, C., Griffiths, P., Hais, M., Healey, S. P., Helmer, E.H., Hostert, P., Lyons, M.B., Meigs, G.W., Pflugmacher, D., Phinn, S.R., Powell, S.L., Scarth, P., Sen, S., Schroeder, T.A., Schneider, A., Sonnenschein, R., Vogelmann, J.E., Wulder, M.A., Zhu, Z., 2014. Bringing an ecological view of change to landsat-based remote sensing. Front. Ecol. Environ. 12, 339–346. https://doi.org/10.1890/130066.

Kennedy, R.E., Yang, Z., Cohen, W.B., 2010. Detecting trends in forest disturbance and recovery using yearly Landsat time series: 1. LandTrendr — Temporal segmentation algorithms. Remote Sens. Environ. 114, 2897–2910. https://doi.org/10.1016/j.rse.2010.07.008.

Kennedy, R.E., Yang, Z., Gorelick, N., Braaten, J., Cavalcante, L., Cohen, W.B., Healey, S., 2018. Implementation of the LandTrendr Algorithm on Google Earth Engine, 10, 691 Remote Sens. 2018 10, 691. https://doi.org/10.3390/RS10050691.

Kozak, A., Munro, D.D., Smith, J.H.G., 1969. Taper functions and their application in forest inventory. For. Chron. 45, 278–283. https://doi.org/10.5558/TFC45278-4.

Krebs, M.A., Reeves, M.C., Baggett, L.S., 2019. Predicting understory vegetation structure in selected western forests of the United States using FIA inventory data. For. Ecol. Manag. 448, 509–527.

Krumlik, J.G., 1974. Biomass and nutrient distribution in two old growth forest ecosystems in south coastal British Columbia. University of British Columbia. https://doi.org/10.14288/1.0075432.

Law, B.E., Berner, L.T., Wolf, C., Ripple, W.J., Trammell, E.J., Birdsey, R.A., 2023. Southern Alaska's forest landscape integrity, habitat, and carbon are critical for meeting climate and conservation goals. AGU Adv. 4, e2023AV000965. https://doi.org/10.1029/2023AV000965.

Lister, A.J., Andersen, H., Frescino, T., Gatziolis, D., Healey, S., Heath, L.S., Liknes, G.C., McRoberts, R., Moisen, G.G., Nelson, M., Riemann, R., Schleeweis, K., Schroeder, T. A., Westfall, J., Wilson, B.T., 2020. Use of remote sensing data to improve the efficiency of national forest inventories: a case study from the United States National Forest Inventory. Forests 11, 1364. https://doi.org/10.3390/f11121364.

Lu, D., Chen, Q., Wang, G., Liu, L., Li, G., Moran, E., 2016. A survey of remote sensing-based aboveground biomass estimation methods in forest ecosystems. Int. J. Digit. Earth 9, 63–105. https://doi.org/10.1080/17538947.2014.990526.

Lucash, M.S., Williams, N.G., Srikrishnan, V., Keller, K., Scheller, R.M., Hegelson, C., Nicholas, R.E., Smithwick, E.A.H., 2023. Balancing multiple forest management objectives under climate change in central Wisconsin, U.S.A. Trees, For. People 14, 100460. https://doi.org/10.1016/j.tfp.2023.100460.

MacKinnon, A., 2003. West coast, temperate, old-growth forests. For. Chron. 79, 475–484. https://doi.org/10.5558/tfc79475-3.

Maltman, J.C., Hermosilla, T., Wulder, M.A., Coops, N.C., White, J.C., 2023. Estimating and mapping forest age across Canada's forested ecosystems. Remote Sens. Environ. 290, 113529. https://doi.org/10.1016/j.rse.2023.113529.

Matasci, G., Hermosilla, T., Wulder, M.A., White, J.C., Coops, N.C., Hobart, G.W., Zald, H.S.J., 2018. Large-area mapping of Canadian boreal forest cover, height, biomass and other structural attributes using Landsat composites and lidar plots. Remote Sens. Environ. 209, 90–106. https://doi.org/10.1016/j.rse.2017.12.020.

McNicol, G., Bulmer, C., D'Amore, D., Sanborn, P., Saunders, S., Giesbrecht, I., Arriola, S. G., Bidlack, A., Butman, D., Buma, B., 2019. Large, climate-sensitive soil carbon stocks mapped with pedology-informed machine learning in the North Pacific coastal temperate rainforest. Environ. Res. Lett. 14, 014004. https://doi.org/10.1088/1748-9326/AAED52.

McRoberts, R.E., 2012. Estimating forest attribute parameters for small areas using nearest neighbors techniques. For. Ecol. Manag., Emerg. Methods Handl. Missing Data For. Ecol. Manag. Appl. 272, 3–12. https://doi.org/10.1016/j.foreco.2011.06.039.

McRoberts, R.E., Næsset, E., Gobakken, T., 2016. The effects of temporal differences between map and ground data on map-assisted estimates of forest area and biomass. Ann. For. Sci. 73, 839–847. https://doi.org/10.1007/s13595-015-0485-6.

McRoberts, R.E., Westfall, J.A., 2014. Effects of uncertainty in model predictions of individual tree volume on large area volume estimates. For. Sci. 60, 34–42. https://doi.org/10.5849/forsci.12-141.

Moeur, M., Stage, A.R., 1995. Most similar neighbor: an improved sampling inference procedure for natural resource planning. Forest science 41, 337–359.

Nowacki, G., Kramer, M., 1998. The Effects of Wind Disturbance on Temperate Rain Forest Structure and Dynamics of Southeast Alaska (General Technical Report No. PNW-GTR-42). USDA Forest Service, Pacific Northwest Research Station.

Nowacki, G.J., Spencer, P., Fleming, M., Brock, T., Jorgenson, T., 2003. Unified ecoregions of Alaska: 2001. US Geological Survey.

Ohmann, J.L., Gregory, M.J., Spies, T.A., 2007. Influence of environment, disturbance, and ownership on forest vegetation of Coastal Oregon. Ecol. Appl. 17, 18–33. https://doi.org/10.1890/1051-0761(2007)017[0018:IOEDAO]2.0.CO;2.

Ohmann, J.L., Gregory, M.J., Henderson, E.B., Roberts, H.M., 2011. Mapping gradients of community composition with nearest-neighbor imputation: extending plot data for landscape analysis. J. Veg. Sci. 22, 660–676. https://doi.org/10.1111/j.1654-1103.2010.01244.x.

Ohmann, J.L., Gregory, M.J., 2002. Predictive mapping of forest composition and structure with direct gradient analysis and nearest-neighbor imputation in coastal Oregon, U.S.A. https://doi.org/10.1139/X02-011.

Ohmann, J.L., Spies, T.A., 1998. Regional gradient analysis and spatial patterns of woody plant communities of oregon forests. Ecol. Monogr. 68, 151–182. https://doi.org/10.1890/0012-9615(1998)068[0151:RGAASP]2.0.CO;2.

Olofsson, P., Foody, G.M., Herold, M., Stehman, S.V., Woodcock, C.E., Wulder, M.A., 2014. Good practices for estimating area and assessing accuracy of land change. Remote Sens. Environ. 148, 42–57. https://doi.org/10.1016/j.rse.2014.02.015.

R Core Team, 2023. R: A Language and Environment for Statistical Computing. R Foundation for Statistical Computing, Vienna, Austria.

Riemann, R., Wilson, B.T., Lister, A., Parks, S., 2010. An effective assessment protocol for continuous geospatial datasets of forest characteristics using USFS Forest Inventory and Analysis (FIA) data. Remote Sens. Environ. 114, 2337–2352. https://doi.org/10.1016/j.rse.2010.05.010.

Santoro, M., Cartus, O., Mermoz, S., Bouvet, A., Le Toan, T., Carvalhais, N., Rozendaal, D., Herold, M., Avitabile, V., Quegan, S., Carreiras, J., Rauste, Y., Balzter, H., Schmullius, C., Seifert, F.M., 2018. A detailed portrait of the forest aboveground biomass pool for the year 2010 obtained from multiple remote sensing observations 18932.

Schulmann, T., Katurji, M., Zawar-Reza, P., 2015. Seeing through shadow: modelling surface irradiance for topographic correction of Landsat ETM+ data. ISPRS J. Photogramm. Remote Sens. 99, 14–24. https://doi.org/10.1016/j.isprsjprs.2014.10.004.

Shanley, C.S., Pyare, S., Goldstein, M.I., Alaback, P.B., Albert, D.M., Beier, C.M., Brinkman, T.J., Edwards, R.T., Hood, E., MacKinnon, A., McPhee, M.V., Patterson, T. M., Suring, L.H., Tallmon, D.A., Wipfli, M.S., 2015. Climate change implications in the northern coastal temperate rainforest of North America. Clim. Change 130, 155–170. https://doi.org/10.1007/s10584-015-1355-9.

Smithwick, E.A.H., Harmon, M.E., Remillard, S.M., Acker, S.A., Franklin, J.F., 2002. Potential upper bounds of carbon stores in forests of the Pacific Northwest. Ecol. Appl. 12, 1303–1317. https://doi.org/10.1890/1051-0761(2002)012[1303:PUBOCS]2.0.CO;2.

Sokolova, M., Lapalme, G., 2009. A systematic analysis of performance measures for classification tasks. Inf. Process. Manag. 45, 427–437. https://doi.org/10.1016/j.ipm.2009.03.002.

Suttles, W., Ames, K., Schoonmaker, P.K., von Hagen, B., Wolf, E.C., 1997. Pre-European history. rain For. home 255–274.

Tadono, T., Nagai, H., Ishida, H., Oda, F., Naito, S., Minakawa, K., Iwamoto, H., 2016. Generation of the 30 m-mesh global digital surface model by ALOS PRISM. Int. Arch. Photogramm., Remote Sens. Spat. Inf. Sci. 41, 157–162.

Ter Braak, C.J.F., 1986. Canonical correspondence analysis: a new eigenvector technique for multivariate direct gradient analysis. Ecology 67, 1167–1179. https://doi.org/10.2307/1938672.

USDA, 2022. U.S. Timber Harvest Boundaries, Alaska.

Veblen, T.T., Alaback, P.B., 1996. A Comparative Review of Forest Dynamics and Disturbance in the Temperate Rainforests of North and South America. Springer, New York, NY, pp. 173–213. https://doi.org/10.1007/978-1-4612-3970-3_9.

Vogeler, J.C., Cohen, W.B., 2016. A review of the role of active remote sensing and data fusion for characterizing forest in wildlife habitat models. Rev. De. TeledetecciónN. 1–14. https://doi.org/10.4995/raet.2016.3981.

Westfall, J.A., Coulston, J.W., Gray, A.N., Shaw, J.D., Radtke, P.J., Walker, D.M., Weiskittel, A.R., MacFarlane, D.W., Affleck, D.L.R., Zhao, D., Temesgen, H., Poudel, K.P., Frank, J.M., Prisley, S.P., Wang, Y., Meador, A.J.S., Auty, D., Domke, G. M., 2024. A national-scale tree volume, biomass, and carbon modeling system for the United States. Gen. Tech. Rep. WO-104. Wash., DC: U. S. Dep. Agric., For. Serv. 104. https://doi.org/10.2737/WO-GTR-104.

White, J.C., Coops, N.C., Wulder, M.A., Vastaranta, M., Hilker, T., Tompalski, P., 2016. Remote sensing technologies for enhancing forest inventories: a review. Can. J. Remote Sens. 42, 619–641. https://doi.org/10.1080/07038992.2016.1207484.

Woodall, C.W., Heath, L.S., Domke, G.M., Nichols, M.C., 2011. Methods and equations for estimating aboveground volume, biomass, and carbon for trees in the U.S. forest inventory, 2010 (No. NRS-GTR-88). U.S. Department of Agriculture, Forest Service, Northern Research Station, Newtown Square, PA. https://doi.org/10.2737/NRS-GTR-88.

Wootten, A., Terando, A., Reich, B.J., Boyles, R.P., Semazzi, F., 2017. Characterizing sources of uncertainty from global climate models and downscaling techniques. J. Appl. Meteorol. Climatol. 56, 3245–3262. https://doi.org/10.1175/JAMC-D-17-0087.1.

Wulder, M.A., Masek, J.G., Cohen, W.B., Loveland, T.R., Woodcock, C.E., 2012. Opening the archive: How free data has enabled the science and monitoring promise of Landsat. Remote Sens. Environ. 122, 2–10. https://doi.org/10.1016/j.rse.2012.01.010.

Yatskov, M.A., Harmon, M.E., Barrett, T.M., Dobelbower, K.R., 2019. Carbon pools and biomass stores in the forests of Coastal Alaska: uncertainty of estimates and impact of disturbance. For. Ecol. Manag. 434, 303–317. https://doi.org/10.1016/J.FORECO.2018.12.014.

Zald, H.S.J., Wulder, M.A., White, J.C., Hilker, T., Hermosilla, T., Hobart, G.W., Coops, N.C., 2016. Integrating Landsat pixel composites and change metrics with lidar plots to predictively map forest structure and aboveground biomass in Saskatchewan, Canada. Remote Sens. Environ. 176, 188–201. https://doi.org/10.1016/j.rse.2016.01.015.